



ELECTRONIC PROPERTIES OF DYE MOLECULES ADSORBED ON  
ANATASE-TITANIA SURFACE FOR SOLAR CELL APPLICATIONS

A THESIS SUBMITTED TO  
THE GRADUATE SCHOOL OF NATURAL AND APPLIED SCIENCES  
OF  
MIDDLE EAST TECHNICAL UNIVERSITY

BY

ENGİN TORUN

IN PARTIAL FULFILLMENT OF THE REQUIREMENTS  
FOR  
THE DEGREE OF MASTER OF SCIENCE  
IN  
PHYSICS

AUGUST 2009

Approval of the thesis:

**ELECTRONIC PROPERTIES OF DYE MOLECULES ADSORBED ON  
ANATASE-TITANIA SURFACE FOR SOLAR CELL APPLICATIONS**

submitted by **ENGİN TORUN** in partial fulfillment of the requirements for the degree of  
**Master of Science in Physics Department, Middle East Technical University** by,

Prof. Dr. Canan Özgen  
Dean, Graduate School of **Natural and Applied Sciences**

\_\_\_\_\_

Prof. Dr. Sinan Bilikmen  
Head of Department, **Physics**

\_\_\_\_\_

Assist. Prof. Dr. Hande Toffoli  
Supervisor, **Physics**

\_\_\_\_\_

Prof. Dr. Şinasi Ellialtıođlu  
Co-supervisor, **Physics**

\_\_\_\_\_

**Examining Committee Members:**

Prof. Dr. Şenay Katırcıođlu  
Physics, METU

\_\_\_\_\_

Assist. Prof. Dr. Hande Toffoli  
Physics, METU

\_\_\_\_\_

Prof. Dr. Şinasi Ellialtıođlu  
Physics, METU

\_\_\_\_\_

Prof. Dr. Mehmet Parlak  
Physics, METU

\_\_\_\_\_

Assoc. Prof. Dr. Ersen Mete  
Physics, Balıkesir University

\_\_\_\_\_

**Date: August 24, 2009**

**I hereby declare that all information in this document has been obtained and presented in accordance with academic rules and ethical conduct. I also declare that, as required by these rules and conduct, I have fully cited and referenced all material and results that are not original to this work.**

Name, Last Name: ENGIN TORUN

Signature :

## ABSTRACT

### ELECTRONIC PROPERTIES OF DYE MOLECULES ADSORBED ON ANATASE-TITANIA SURFACE FOR SOLAR CELL APPLICATIONS

Torun, Engin

M.S., Department of Physics

Supervisor : Yrd. Doç. Dr. Hande TOFFOLI

Co-Supervisor : Prof. Dr. Şinasi Ellialtıođlu

August 2009, 59 pages

Wide band gap metal oxides have recently become one of the most investigated materials in surface science. Among these metal oxides especially  $\text{TiO}_2$  attracts great interest, because of its wide range applications, low cost, biocompatibility and ease of analysis by all experimental techniques. The usage of  $\text{TiO}_2$  as a component in solar cell technology is one of the most investigated applications of  $\text{TiO}_2$ . The wide band gap of  $\text{TiO}_2$  renders it inefficient for isolated use in solar cells.  $\text{TiO}_2$  surface are therefore coated with a dye in order to increase efficiency. This type of solar cells are called dye sensitized solar cells .

The efficiency of dye sensitized solar cells is directly related with the absorbed light portion of the entire solar spectrum by the dye molecule. In spite of the early dyes, recent dye molecules, which are called wider wavelength response dye molecules, can absorb a larger portion of entire solar spectrum. Thus, the efficiency of dye sensitized solar cells is increased by a considerably amount.

In this thesis the electronic structure of organic rings, which are the fundamental components of the dye molecules, adsorbed on anatase (001) surface is analyzed using density functional

theory. The main goal is to obtain a trend in the electronic structure of the system as a function of increasing ring number. Electronic structure analysis is conducted through band structure and density of states calculations. Results are presented and discussed in the framework of dye sensitized solar cells theory.

Keywords: density functional theory , dye sensitized solar cells , organic rings, titanium dioxide, anatase

# ÖZ

## GÜNEŞ PİLİ UYGULAMALARI İÇİN BOYA MOLEKÜLLERİ ADSORBE EDİLMİŞ ANATAZ-TİTANYA YÜZEYİNİN ELEKTRONİK ÖZELLİKLERİ

Torun, Engin

Yüksek Lisans, Fizik Bölümü Bölümü

Tez Yöneticisi : Yrd. Doç. Dr. Hande TOFFOLI

Ortak Tez Yöneticisi : Prof. Dr. Şinasi Ellialtıođlu

Ađustos 2009, 59 sayfa

Geniş bant aralıklı metal oksitler yüzey bilimde son zamanlarda üzerinde en çok çalışılan malzeme olmaya başlamıştır. Bu metal oksitler arasında en büyük ilgiyi, geniş uygulama alanları, düşük maliyet, bio-uyumluluk ve bütün deneysel tekniklerle kolaylıkla incelenebilmesi gibi özellikleri nedeni ile  $TiO_2$  çekmektedir.  $TiO_2$  'nin en yoğun olarak konu edildiđi alanların başında güneş pili kullanımı gelmektedir. Geniş bant aralığı nedeni ile verimliliđi yetersiz bulunan  $TiO_2$  'nin verimini artırmak için  $TiO_2$  yüzeyi ışık harmanlayıcı boya maddesi ile kaplanması gerekmektedir. Bu tür güneş pillerine boya sentezli güneş pilleri denmektedir.

Güneş pillerinin verimliliđi, boya maddesinin güneş spektumunun ne kadarını absorbe ettiđi ile ilişkilidir. Geçmişte kullanılan boya maddelerinin aksine, geniş dalga boyuna duyarlı boya maddeleri güneş spektumunun daha büyük bir miktarını absorbe etmektedir. Bu nedenle, boya sentezli güneş pillerinin verimliliđi önemli ölçüde artmıştır.

Bu tezde  $TiO_2$  anataz (001) yüzeyine bağlanmış, boya maddelerinin bileşenlerinden biri olan organik moleküllerin elektronik özellikleri yoğunluk fonksiyoneli teorisi(DFT) ile incelenmiştir. Bu işteki asıl amaç sistemin elektronik özelliklerinde artan halka sayısına göre bir trend yakalamaya çalışmaktır. Sistemlerin elektronik özellikleri bant yapıları ve fiziksel durum

yoğunluđu yardımı ile incelenmiş, sonuçlar boya sentezli güneş pilleri teorisi çerçevesinde tartışılmıştır.

Anahtar Kelimeler: yoğunluk fonksiyoneli teorisi, boya sentezli güneş pilleri, organik moleküller, titanyum dioksit, anataz

*To my family*

## ACKNOWLEDGMENTS

I would like to express my thanks to my supervisor Hande Toffoli for her guidance, encouragement and willing to help me all the time throughout my master's period.

I also would like to thank my co-supervisor Şinasi Ellialtıođlu for his help and support, also I would like to thank Ersen Mete for his valuable ideas and discussions.

I would like to express my gratitude to my friends, Özge, Turkan, Ender, Burak, Derya, Sermin. I wish to give my special thanks to my family for the moral support and patience during my study. I am also grateful to Duygu, for her support, patience and understanding during the writing of this thesis.

This work is financially supported by TÜBİTAK, The Scientific and Technological Research Council of Turkey (Grant no: TBAG 107T560).



2.5.4	Density in terms of planewaves . . . . .	22
2.6	EXCHANGE and CORRELATION ENERGY FUNCTIONALS . . .	23
2.6.1	The Local density approximation . . . . .	23
2.6.2	The Generalized gradient approximation . . . . .	24
2.7	PSEUDOPOTENTIAL . . . . .	24
2.7.1	Norm-conserving pseudopotential . . . . .	25
2.7.2	Ultrasoft pseudopotentials . . . . .	26
3	ELECTRONIC STRUCTURE ANALYSIS OF TiO <sub>2</sub> (001) ANATASE SUR- FACE . . . . .	27
3.1	APPLICATION OF TiO <sub>2</sub> . . . . .	27
3.1.1	Photocatalysis application . . . . .	27
3.1.2	Solar cell applications . . . . .	28
3.2	DENSITY FUNCTIONAL THEORY CALCULATIONS OF ANATASE (001) SURFACE . . . . .	29
3.2.1	Crystal structure of TiO <sub>2</sub> . . . . .	29
3.2.1.1	Rutile . . . . .	29
3.2.1.2	Anatase . . . . .	30
3.2.1.3	Brookite . . . . .	30
3.2.2	Bulk calculations . . . . .	31
3.2.3	Surface calculations . . . . .	33
4	ELECTRONIC STRUCTURE ANALYSIS OF AROMATIC MOLECULES, ADSORBED ON TiO <sub>2</sub> (001) ANATASE SURFACE . . . . .	36
4.1	ADSORPTION OF ANCHOR GROUP MOLECULES . . . . .	36
4.1.1	Formic acid adsorption . . . . .	36
4.1.2	Phosphonic acid adsorption . . . . .	39
4.2	AROMATIC RING ADSORPTION ON ANATASE (001) SURFACE	42
4.2.1	Adsorption of aromatic rings anchored by formic acid . . .	42
4.2.2	Adsorption of aromatic rings anchored by phosphonic acid	46
5	CONCLUSION . . . . .	54
	REFERENCES . . . . .	56

## LIST OF TABLES

### TABLES

Table 4.1	Binding energy and the gaps for each system with formic acid as the anchor.	47
Table 4.2	Binding energy and the gaps for each system with phosphonic acid as the anchor . . . . .	51

## LIST OF FIGURES

### FIGURES

Figure 3.1 Unit cell of TiO <sub>2</sub> in rutile form, (a) front view, (b) side view, and (c) top view	30
Figure 3.2 Unit cell of TiO <sub>2</sub> in anatase form, (a) front view, (b) side view, and (c) top view . . . . .	30
Figure 3.3 Unit cell of TiO <sub>2</sub> in brookite form, (a) front view, (b) side view, and (c) top view . . . . .	31
Figure 3.4 Projected band structure of anatase bulk . . . . .	32
Figure 3.5 The anatase slab which is used in this work a) Front view, b) Side view, c) Top view . . . . .	34
Figure 3.6 Distance between oxygen atom and the titanium atoms at the surface of slab (a) before and (b) after relaxation . . . . .	35
Figure 3.7 Anatase (001) surface bands projected on bulk band structure . . . . .	35
Figure 3.8 Partial charge densities of surface states at $\Gamma$ . . . . .	35
Figure 4.1 Formic acid molecule (a) front view, (b) side view and c) top view. . . . .	37
Figure 4.2 Formic acid adsorption on TiO <sub>2</sub> anatase (001) 2 × 2 surface (a) front view (b) side view and (c) top view. . . . .	37
Figure 4.3 Band structure along the symmetry lines of the surface Brillouin zone and density of states of (a) clean TiO <sub>2</sub> surface (b) formic acid adsorbed on anatase (001) surface. Shaded region shows the bulk band projected on the same surface Brillouin zone. The top of the bulk valence band is taken to be zero. . . . .	38
Figure 4.4 Density of states of the whole system (blue line) and the partial density of states due to the formic acid (shaded in red) . . . . .	39
Figure 4.5 Phosphonic acid a) Front view b) Side view c) Top view . . . . .	40

Figure 4.6 Phosphonic acid adsorption on TiO <sub>2</sub> anatase (001) surface. (a) Front view, (b) side view, and c) top view . . . . .	40
Figure 4.7 Band structure along the symmetry lines of the surface Brillouin zone and density of states of (a) Clean surface and (b) Phosphonic acid adsorbed on anatase (001) surface. Shaded region shows the bulk band projected on the same surface Brillouin zone. The top of the bulk valence band is taken to be zero. . . . .	41
Figure 4.8 Density of states of the whole system (blue line) and the partial density of states due to the phosphonic acid (shaded in red). . . . .	41
Figure 4.9 Charge density plots for (a) the upper lying gap state and (b) the lower lying gap state. . . . .	41
Figure 4.10 Geometry optimized TiO <sub>2</sub> anatase (001) 2×2 surfaces with varying number of aromatic rings anchored via formic acid . . . . .	43
Figure 4.11 Band Structures of aromatic ring adsorption on anatase (001) surface anchored via formic acid. (a) Formic acid adsorbed system, and the number of rings in figures (b), (c), (d), (e), (f) are 1, 2, 3, 4, 5 respectively . . . . .	44
Figure 4.12 Partial charge densities for the gap states at $\Gamma$ point. The number of rings in figure (a) , (b), (c), (d), (e) are 1, 2, 3, 4, 5 respectively. The first plot in (b) and (c) corresponds to the upper lying gap state, the second one corresponds to the lower lying gap state. In (d) and (e) the first plot corresponds to the upper lying gap state, the second one corresponds to the state which is in the middle and the third one corresponds to the lower lying gap state . . . . .	45
Figure 4.13 HOMO–LUMO energy differences of adsorbed molecules versus the number of aromatic rings . . . . .	46
Figure 4.14 Contribution of molecule’s partial density of states to the total density of states. Valence band top of the bulk projection is at 0 eV. The number of rings in figure (a), (b), (c), (d), (e) are 1, 2, 3, 4, 5 respectively. The HOMO and the LUMO level of the isolated rings is shown above the each of the panel. . . . .	48
Figure 4.15 Geometry optimized TiO <sub>2</sub> anatase (001) 2×2 surfaces with varying number of aromatic rings anchored via phosphonic acid . . . . .	49

Figure 4.16 Band Structures of aromatic ring adsorption on anatase (001) surface anchored via phosphonic acid. (a) Phosphonic acid adsorbed system, and the number of rings in figures (b), (c), (d), (e), (f) are 1, 2, 3, 4, 5 respectively . . . . .	49
Figure 4.17 Partial charge densities for the gap states at $\Gamma$ point. The number of rings in figure a,b,c,d,e are 1,2,3,4,5 respectively. The first plot in a, corresponds to upper lying gap state in Fig. 4.16(b), the second and the third one corresponds to middle gap state and the final one corresponds to lower lying gap state. The plots in figure b,c,d,e are the partial charge densities of gap states in Fig. 4.16(c),(d),(e) and ordered as above respectively . . . . .	50
Figure 4.18 Contribution of molecule's partial density of states to the total density of states. Valence band top of the bulk projection is at 0 eV. The number of rings in figure (a), (b), (c), (d), (e) are 1, 2, 3, 4, 5 respectively. The HOMO and the LUMO level of the isolated rings is shown above the each of the panel. . . . .	52
Figure 4.19 HOMO-LUMO energy difference of adsorbed aromatic rings . . . . .	53
Figure 4.20 Variation energy difference between HOMO-CBE of the systems versus number of rings . . . . .	53
Figure 4.21 Energy difference between HOMO-LUMO gap of the systems versus number of rings . . . . .	53

# CHAPTER 1

## INTRODUCTION

Due to their wide range of applications, experimental and theoretical studies on wide band gap metal oxides have gained acceleration in recent years. Among these wide band gap metal oxides  $\text{TiO}_2$  has become one of the most investigated materials in surface science. Its wide range of applications, low cost, biocompatibility and ease of analysis by all experimental techniques make  $\text{TiO}_2$  a desirable metal oxide.  $\text{TiO}_2$  is used mostly in photocatalytic applications, solar cell applications and electric devices, in addition it is used as a gas sensor, white pigments, biomaterials, memory devices and optical coatings [1, 2].

One of the most investigated applications of  $\text{TiO}_2$  is its usage as a component in solar cell technology. Due to its wide band gap,  $\text{TiO}_2$  absorbs light in the near ultraviolet region. This is a disadvantage for solar cell applications because this region is a small portion of the entire solar spectrum. In order to increase its efficiency  $\text{TiO}_2$  should be coated with light harvesting dye materials [3, 4]. This kind of solar cell is called dye sensitized solar cells and it was first investigated by Grätzel using a few nanometers of  $\text{TiO}_2$  coated with a low cost light harvesting dye molecules, for this reason the dye sensitized solar cells is also known as the Grätzel cell [5].

The efficiency of conversion of solar energy to electric energy in a dye sensitized solar cell is mostly proportional to the efficiency of the light harvesting dye coating the molecule underneath. Early dyes, were sensitive to photons which are in the blue and ultraviolet region. However, recent studies show that the efficiency of dye sensitized solar cells is increased by a considerable amount by introducing wider wavelength response dye molecules. The wider wavelength response dye molecules are very important for efficiency of dye sensitized solar cells because they can absorb a larger portion of the solar spectrum than one wavelength sensitive dye molecules so they have higher solar energy to electric energy conversion efficiency

[6, 7].

Another important issue to consider while constructing dye sensitized solar cells is the particular form of  $\text{TiO}_2$  used, since some  $\text{TiO}_2$  polymorphs do not have photocatalysis and photovoltaic properties. In nature,  $\text{TiO}_2$  can be found in mainly three different crystal structures: rutile, anatase and brookite. Rutile is the most stable crystal form of  $\text{TiO}_2$ , while the other crystal forms can be converted to rutile by heating. Another crystal form of  $\text{TiO}_2$  is anatase, which is widely used in photovoltaic devices because  $\text{TiO}_2$  nanoparticles are formed in metastable anatase form instead of more stable rutile form. Unlike the other forms brookite does not have photovoltaic and photocatalysis properties and it is rarely found in nature [1, 2].

The surfaces of most crystals are often found to enrich the material properties by introducing new aspects. Especially, when the size of the material is decreased, the surface properties appear more dominantly than the bulk properties. For instance, the photovoltaic and photocatalysis properties of  $\text{TiO}_2$  emerge more clearly when  $\text{TiO}_2$  forms as nanomaterials. In addition, the surface properties of materials change when the facet of the surface changes, for example the most stable facet of anatase form of  $\text{TiO}_2$  is (101) surface, however the most active facet of it is (001) surface. Thus, in photovoltaic and photocatalysis devices anatase (001) surface is widely used [2, 8, 9].

In the light of above discussions, in this thesis the electronic structure of organic rings, which are the components of dye molecules, adsorbed on  $\text{TiO}_2$  anatase (001) surface is investigated by using density functional theory (DFT). The organic rings are so inert that they can be bonded to the surface only through anchor group molecules. Formic acid ( $\text{RCOOH}$ ) and phosphonic acid ( $\text{RPO}_3\text{H}_2$ ), which are the most widely used anchor group molecules are used as examples in this thesis. These anchors are adsorbed on surfaces with high binding energy and they have ultrafast electron transfer property, favoring their usage as the anchor molecules in this and other [2, 3, 6] studies. The electronic structure of the organic molecules which have one to five rings adsorbed on  $\text{TiO}_2$  anatase [001] surface using two anchors is analyzed separately. The aim of this work is to obtain a trend in the electronic property of organic molecules as a function of number of rings [4, 10].

This thesis is composed of five chapters. The second chapter is a brief description of the theoretical method, namely DFT. In the third chapter, the crystal properties of  $\text{TiO}_2$  and DFT calculations on bulk anatase and its [001] surface are introduced. In chapter four, the electronic

structure calculation results of linear series organic rings are given. The thesis is concluded in chapter five with conclusion and future works.

## CHAPTER 2

### DENSITY FUNCTIONAL THEORY

In physics, in order to understand the electronic structure of matter there are lots of approaches such as tight binding, hartree-fock or free electron model. DFT is one of the most popular quantum mechanical approaches to matter among them, it is used to calculate the binding energy of molecules, band structure of crystals, superconductivity and magnetic properties of matters successfully [11].

#### 2.1 MANY-BODY HAMILTONIAN

To obtain information about a physical system the wavefunction of that system should be found. The wavefunction can be calculated by solving Schrödinger's equation [12].

$$\hat{H}\psi(\vec{r}) = E\psi(\vec{r}) \quad (2.1)$$

For the simplest case, if an electron is moving under influence of coulombic potential, the Schrödinger's equation become.

$$-\left[ \frac{\hbar^2}{2m_e} \nabla_{\vec{r}}^2 + \frac{e^2}{4\pi\epsilon_0 r} \right] \psi(\vec{r}) = E\psi(\vec{r}) \quad (2.2)$$

In this case, this wavefunction can be written easily. However, bigger systems such as atoms other than hydrogen atom as well as molecules and solids are analyzed, this wavefunction can not be written so easily. In order to get many-body Hamiltonian some extra terms should be added to the single body Hamiltonian. Then, using many-body Hamiltonian the Schrödinger's equation should be solved to find the wavefunction of system. For the general case the many-body Hamiltonian has two parts:

$$\hat{H} = \hat{T} + \hat{V} \quad (2.3)$$

The kinetic energy of the particles  $\hat{T}$  and the potential energy  $\hat{V}$ , which includes the interaction energy of the particles in the system.

The kinetic energy part contains the sum of kinetic energies of electrons and nuclei. However, the nucleus is hundreds times heavier than electrons, so if there is a change in the position of nucleus the electrons can arrange themselves immediately to the new position of nucleus. It means that change in position of nuclei do not effect the electrons so their contribution to kinetic energy term is neglected. This is called Born-Oppenheimer approximation [13].

The potential energy term contains three kinds of interactions; nucleus-nucleus , nucleus-electron , electron-electron interaction.

It is assumed that the nuclei are classical particles in nucleus-nucleus interaction, and they interact with Coulombic forces. The nucleus-electron interaction is also a Coulombic interaction; it is assumed that each electron interacts with nucleus separately. This part is replaced by pseudopotentials in practise in DFT. The electron-electron interaction part is the part that makes many-body Hamiltonian hard to handle and it is also a Coulombic interaction. The electronic calculation methods are utilized to make this part simpler. The quality of calculation is mainly based on how well this part is approximated.

Considering above information, the many-body Hamiltonian can be written in a closed form

$$\hat{H} = \hat{T}_e + \hat{V}_{ne} + \hat{V}_{ee} + \hat{V}_{nn} \quad (2.4)$$

There are  $N_e$  electrons and  $N_n$  nuclei in the system then the kinetic energy part of many-body Hamiltonian is [14]

$$\hat{T}_e = -\frac{\hbar^2}{2m_e} \sum_i^{N_e} \nabla_i^2 \quad (2.5)$$

The nucleus-electron interaction in the potential part is written as

$$\hat{V}_{ne} = -\frac{1}{4\pi\epsilon_0} \sum_I^{N_n} \sum_i^{N_e} \frac{Q_I e}{|\vec{r}_i - \vec{R}_I|} \quad (2.6)$$

here  $\vec{r}_i$  defines the position of electrons and  $\vec{R}_I$  defines the position of nuclei also  $Q_I = Z_I e$ . There are  $N_n$  nuclei and  $N_e$  electrons in the system so the total interaction is obtained by summing up all the one to one interaction. The rest of the terms in the potential part  $\hat{V}_{ee}$  and

$\hat{V}_{mn}$  are simple Coulombic interactions

$$\hat{V}_{ee} = \frac{1}{2} \frac{e^2}{4\pi\epsilon_0} \sum_i^{Ne} \sum_{j \neq i}^{Ne} \frac{1}{|\vec{r}_i - \vec{r}_j|} \quad (2.7a)$$

$$\hat{V}_{nn} = \frac{1}{2} \frac{e^2}{4\pi\epsilon_0} \sum_I^{Nn} \sum_{J \neq I}^{Nn} \frac{Z_I Z_J}{|\vec{R}_I - \vec{R}_J|} \quad (2.7b)$$

The nuclei do not interact with themselves. Thus, in the inner sum the  $i = j$  and  $I = J$  terms are excluded. Also  $\frac{1}{|\vec{r}_i - \vec{r}_j|}$  and  $\frac{1}{|\vec{r}_j - \vec{r}_i|}$  terms are the same, however, in the above sum both of them are counted which is incorrect, so  $\frac{1}{2}$  factor is introduced to exclude the self interaction. Same consideration holds for the second equation as well. Finally, everything can be put together to get the many-body Hamiltonian .

$$\hat{H} = -\frac{\hbar^2}{2m_e} \sum_i^{Ne} \nabla_i^2 + \frac{e^2}{4\pi\epsilon_0} \left[ -\sum_I^{Nn} \sum_i^{Ne} \frac{Z_I}{|\vec{r}_i - \vec{R}_I|} + \frac{1}{2} \sum_i^{Ne} \sum_{j \neq i}^{Ne} \frac{1}{|\vec{r}_i - \vec{r}_j|} + \frac{1}{2} \sum_I^{Nn} \sum_{J \neq I}^{Nn} \frac{Z_I Z_J}{|\vec{R}_I - \vec{R}_J|} \right] \quad (2.8)$$

This equation seems crowded due to the usage of SI units, where energy is in Joule and length is in meters. When atomic units are used, where energy is in Hartree and the length is in Bohr, this equation becomes much simpler. A Hartree is defined as ground state energy of an electron in the hydrogen atom and a Bohr is its average ground state radius [15].

$$a_0 = \frac{4\pi\epsilon_0 \hbar^2}{m_e e^2} \quad (2.9a)$$

$$E_h = \frac{\hbar^2}{m_e a_0^2} = \frac{e^2}{4\pi\epsilon_0} \quad (2.9b)$$

In order to rescale the many-body Hamiltonian by  $a_0$ ,  $\frac{1}{|r-r'|}$  should be replaced with  $\frac{1}{a_0|r-r'|}$  and the Laplacian operator in kinetic energy term will should be replaced with  $\frac{\nabla^2}{a_0^2}$ . Then the many-body Hamiltonian becomes,

$$\hat{H} = -\frac{\hbar^2}{2m_e a_0^2} \sum_i^{Ne} \nabla_i^2 + \frac{e^2}{4\pi\epsilon_0 a_0} \left[ -\sum_I^{Nn} \sum_i^{Ne} \frac{Z_I}{|\vec{r}_i - \vec{R}_I|} + \frac{1}{2} \sum_i^{Ne} \sum_{j \neq i}^{Ne} \frac{1}{|\vec{r}_i - \vec{r}_j|} + \frac{1}{2} \sum_I^{Nn} \sum_{J \neq I}^{Nn} \frac{Z_I Z_J}{|\vec{R}_I - \vec{R}_J|} \right] \quad (2.10)$$

If the second constant is divided and multiplied by  $\frac{m_e}{\hbar^2}$  and Eq. 2.9 is used then many-body Hamiltonian will be

$$\hat{H} = E_H \hat{H} \quad (2.11)$$

The hamiltonian is rescaled by  $E_H$  and the new Hamiltonian becomes  $\hat{H}$  finally, the rescaled hamiltonian in atomic units is,

$$\hat{H} = -\frac{1}{2} \sum_i^{Ne} \nabla_i^2 - \sum_I^{Nn} \sum_i^{Ne} \frac{Z_I}{|\vec{r}_i - \vec{R}_I|} + \frac{1}{2} \sum_i^{Ne} \sum_{j \neq i}^{Ne} \frac{1}{|\vec{r}_i - \vec{r}_j|} + \frac{1}{2} \sum_I^{Nn} \sum_{J \neq I}^{Nn} \frac{Z_I Z_J}{|\vec{R}_I - \vec{R}_J|} \quad (2.12)$$

The many-body Hamiltonian is simplified by writing it in atomic units but its exact solution is still impossible to get. In order to find the solution of many-body Hamiltonian there are two basic classes of methods in literature; density based approaches and wavefunction based approaches, DFT approach is one of the best density based approaches .

## 2.2 TOTAL ENERGY IN TERMS OF DENSITY

It was stated before that solving many-body Schrödinger equation for ground state energy and ground state wavefunction is impossible to handle for some systems. The aim in DFT is to eliminate wavefunction dependence by writing all terms in terms of density.

### 2.2.1 Definition of density

Electron density  $n(\vec{r})$  is the fundamental observable of the system and it can be found using single-particle density operator.

$$\hat{n}(\vec{r}) = \sum_{i=1,N} \delta(\vec{r} - \vec{r}_i) \quad (2.13)$$

to find the density the expectation value of this operator should be found using many body wavefunction.

$$n(\vec{r}) = \langle \psi | \hat{n}(\vec{r}) | \psi \rangle = \sum_{i=1,N} \int \delta(\vec{r} - \vec{r}_i) |\psi(\vec{r}_1, \dots, \vec{r}_N)|^2 d\vec{r}_1 \dots d\vec{r}_N \quad (2.14)$$

using the properties of dirac delta function Eq. 2.14 can be written as:

$$n(\vec{r}) = \int |\psi(\vec{r}, \vec{r}_2, \dots, \vec{r}_N)|^2 d\vec{r}_2 d\vec{r}_3 \dots d\vec{r}_N + \int |\psi(\vec{r}_1, \vec{r}, \dots, \vec{r}_N)|^2 d\vec{r}_1 d\vec{r}_3 \dots d\vec{r}_N + \dots \quad (2.15)$$

In Eq. 2.15 there are N same integral so;

$$n(\vec{r}) = N \int |\psi(\vec{r}, \vec{r}_2, \dots, \vec{r}_N)|^2 d\vec{r}_2 d\vec{r}_3 \dots d\vec{r}_N \quad (2.16)$$

here  $\vec{r}$  represents position of each electron. Also integrating the density over all space will give the number of electrons.

$$\int d\vec{r} n(\vec{r}) = N \quad (2.17)$$

assuming that the wavefunction is normalized.

### 2.2.2 Energy in terms of density

As it was mentioned before the many-body Hamiltonian for a many-body system was

$$\hat{H} = \hat{T}_e + \hat{V}_{ne} + \hat{V}_{ee} + \hat{V}_{nn} \quad (2.18)$$

If the last term is taken as a constant, the electronic Hamiltonian is

$$\hat{H}_e = \hat{T}_e + \hat{V}_{ne} + \hat{V}_{ee} \quad (2.19)$$

In atomic units electronic Hamiltonian can be written as,

$$\hat{H}_e = -\frac{1}{2} \sum_i^{N_e} \nabla_i^2 - \sum_I^{N_n} \sum_i^{N_e} \frac{Z_I}{|\vec{r}_i - \vec{R}_I|} + \frac{1}{2} \sum_i^{N_e} \sum_{j \neq i}^{N_e} \frac{1}{|\vec{r}_i - \vec{r}_j|} \quad (2.20)$$

The energy value of this electronic hamiltonian can be found by calculating the expectation value of it. The expectation value of  $\hat{H}_e$  is calculated using many body wavefunction and it is assumed that this many body wavefunction is calculated from many-body Schrödinger equation .

$$\langle \psi(\vec{r}_1, \dots, \vec{r}_n) | \hat{H}_e | \psi(\vec{r}_1, \dots, \vec{r}_n) \rangle = \langle \psi(\vec{r}_1, \dots, \vec{r}_n) | \hat{T}_e + \hat{V}_{ne} + \hat{V}_{ee} | \psi(\vec{r}_1, \dots, \vec{r}_n) \rangle \quad (2.21)$$

This expectation value can be written as

$$\begin{aligned} \langle \psi(\vec{r}_1, \dots, \vec{r}_n) | \hat{H}_e | \psi(\vec{r}_1, \dots, \vec{r}_n) \rangle &= \langle \psi(\vec{r}_1, \dots, \vec{r}_n) | \hat{T}_e | \psi(\vec{r}_1, \dots, \vec{r}_n) \rangle + \langle \psi(\vec{r}_1, \dots, \vec{r}_n) | \hat{V}_{ne} | \psi(\vec{r}_1, \dots, \vec{r}_n) \rangle \\ &\quad + \langle \psi(\vec{r}_1, \dots, \vec{r}_n) | \hat{V}_{ee} | \psi(\vec{r}_1, \dots, \vec{r}_n) \rangle \end{aligned} \quad (2.22)$$

and it can be written in terms of density term by term. The first term, which is kinetic energy, has second order derivative so it is hard to collect the wavefunction and its conjugate to form a simple norm square.

$$\langle \psi(\vec{r}_1, \dots, \vec{r}_n) | \hat{T}_e | \psi(\vec{r}_1, \dots, \vec{r}_n) \rangle = -\frac{1}{2} \sum_i^{N_e} \int \psi(\vec{r}_1, \dots, \vec{r}_n) \nabla_i^2 \psi(\vec{r}_1, \dots, \vec{r}_n) \quad (2.23)$$

To write the kinetic energy term in terms of density an important assumption is made, which is that the density can be written in terms of single particle orbitals  $\phi_n(\vec{r})$ .

$$n(\vec{r}) = \sum_n^{N_e} |\phi_n(\vec{r})|^2 \quad (2.24)$$

Eq. 2.24 says that instead of considering the system as a many body system, it can be considered as collection of single particles. Thus, the density of many body system can be written in terms of single body orbitals. Note that, the ground state density of the collection of single particle system is the same as the real system. These single particle orbitals are called Kohn-Sham orbitals and they are formed using slater determinant.

### 2.2.2.1 Slater determinant

Using Kohn-Sham orbitals the simplest many body wavefunction can be written as

$$\Psi(\vec{x}_1, \vec{x}_2, \dots, \vec{x}_N) = \phi_1(\vec{x}_1)\phi_2(\vec{x}_2)\dots\phi_N(\vec{x}_N) \quad (2.25)$$

For the generality the  $\vec{x}_i$  is the generalized coordinate which contains spin part and spatial part. However, this wavefunction is not satisfactory for the fermions because it fails to satisfy antisymmetry condition. This condition states that fermion wavefunction change sign under odd permutations.

$$\hat{P}_{ij}\Psi(\vec{x}_1, \dots, \vec{x}_i, \vec{x}_j, \dots, \vec{x}_N) = \Psi(\vec{x}_1, \dots, \vec{x}_j, \vec{x}_i, \dots, \vec{x}_N) = -\Psi(\vec{x}_1, \dots, \vec{x}_i, \vec{x}_j, \dots, \vec{x}_N) \quad (2.26)$$

Here  $\hat{P}_{ij}$  is permutation operator. This condition will be satisfied when many body wavefunction is written as a determinant which is called Slater determinant [16].

$$\Psi(\vec{x}_1, \vec{x}_2, \dots, \vec{x}_N) = \frac{1}{\sqrt{N!}} \begin{vmatrix} \phi_1(\vec{x}_1) & \phi_2(\vec{x}_1) & \dots & \phi_N(\vec{x}_1) \\ \phi_1(\vec{x}_2) & \phi_2(\vec{x}_2) & \dots & \phi_N(\vec{x}_2) \\ \vdots & \vdots & \vdots & \vdots \\ \phi_1(\vec{x}_N) & \phi_2(\vec{x}_N) & \dots & \phi_N(\vec{x}_N) \end{vmatrix} \quad (2.27)$$

This determinant can be written as

$$\sum_i^{N!} (-1)^{P(i_1, i_2, \dots, i_N)} \phi_{i_1}(\vec{x}_1)\phi_{i_2}(\vec{x}_2)\dots\phi_{i_N}(\vec{x}_N) \quad (2.28)$$

and the wavefunction becomes

$$\Psi(\vec{x}_1, \vec{x}_2, \dots, \vec{x}_N) = -\frac{1}{\sqrt{N!}} \sum_i^{N!} (-1)^{P(i_1, i_2, \dots, i_N)} \phi_{i_1}(\vec{x}_1)\phi_{i_2}(\vec{x}_2)\dots\phi_{i_N}(\vec{x}_N) \quad (2.29)$$

There is  $N!$  terms in the determinant so the sum runs from one to  $N!$  and each one is multiplied by one or minus one depending on the parity of the permutation. If it is odd permutation then the terms get a minus one in front of them and if it is even then the constant will be one. Thus, the wavefunction satisfies the antisymmetry conditions when it is written as Slater determinant.

Due to the derivative in the kinetic energy term, it can not be written in terms of density but it can be written in terms of Kohn-Sham orbitals by using the assumption in Eq.2.24.

$$T = -\frac{1}{2} \sum_n^{N_e} \int d\vec{r} \phi_n^*(\vec{r}) \nabla^2 \phi_n(\vec{r}) + \Delta T \quad (2.30)$$

The kinetic energies of Kohn-Sham orbitals obviously are not equal to the real many body kinetic energy. Thus, the kinetic energy term is written in terms of single particle kinetic energy term and a correction. When the energy is tried to be minimized with respect to density this will not be a problem since minimization with respect to complex conjugates of Kohn-Sham orbitals will be equal to the minimization with respect to density.

The second term in the electronic Hamiltonian which should be written in terms of density is the nucleus electron potential energy. This has no derivative so the wavefunction and its conjugate can be written as a simple norm-square.

$$\langle \psi(\vec{r}_1, \dots, \vec{r}_N) | \hat{V}_{ne} | \psi(\vec{r}_1, \dots, \vec{r}_N) \rangle = E_{ne} = - \sum_i^{N_e} \sum_I^{N_n} \int \frac{Z_I}{|\vec{r}_i - \vec{R}_I|} |\psi(\vec{r}_1, \dots, \vec{r}_N)|^2 d\vec{r}_1 \dots d\vec{r}_N \quad (2.31)$$

It can be expanded over electron index

$$E_{ne} = - \sum_I^{N_e} \left[ \int \frac{Z_I}{|\vec{r}_1 - \vec{R}_I|} |\psi(\vec{r}_1, \dots, \vec{r}_N)|^2 d\vec{r}_1 d\vec{r}_2 \dots d\vec{r}_N + \int \frac{Z_I}{|\vec{r}_2 - \vec{R}_I|} |\psi(\vec{r}_1, \dots, \vec{r}_N)|^2 d\vec{r}_1 d\vec{r}_2 \dots d\vec{r}_N + \dots \right] \quad (2.32)$$

These integrals can be seperated

$$E_{ne} = - \sum_I^{N_e} \left[ \int \frac{Z_I}{|\vec{r}_1 - \vec{R}_I|} d\vec{r}_1 \int |\psi(\vec{r}_1, \dots, \vec{r}_N)|^2 d\vec{r}_2 d\vec{r}_3 \dots d\vec{r}_N + \int \frac{Z_I}{|\vec{r}_2 - \vec{R}_I|} d\vec{r}_2 \int |\psi(\vec{r}_1, \dots, \vec{r}_N)|^2 d\vec{r}_1 d\vec{r}_3 \dots d\vec{r}_N + \dots \right] \quad (2.33)$$

The second integral at each term is the definition of density so this equation can be written as

$$E_{ne} = - \frac{1}{N_e} \sum_I^{N_e} \left[ \int \frac{Z_I}{|\vec{r}_1 - \vec{R}_I|} d\vec{r}_1 n(\vec{r}_1) + \int \frac{Z_I}{|\vec{r}_2 - \vec{R}_I|} d\vec{r}_2 n(\vec{r}_2) + \dots \right] \quad (2.34)$$

It is assumed that the  $\vec{r}_i$  values can be replaced by dummy variables so all density terms becomes equal.

$$E_{ne} = - \sum_I^{N_e} \int n(\vec{r}) \frac{Z_I}{|\vec{r} - \vec{R}_I|} d\vec{r} = \int n(\vec{r}) V_{ne}(\vec{r}) d\vec{r} \quad (2.35)$$

The final term in the electronic Hamiltonian which should be written in terms of density is the electron electron potential energy term.

$$\langle \psi(\vec{r}_1, \dots, \vec{r}_N) | \hat{V}_{ee} | \psi(\vec{r}_1, \dots, \vec{r}_N) \rangle = E_{ee} = \sum_i^{N_e} \sum_{i \neq j}^{N_e} \int \frac{1}{|\vec{r}_i - \vec{r}_j|} |\psi(\vec{r}_1, \dots, \vec{r}_N)|^2 d\vec{r}_1 \dots d\vec{r}_N \quad (2.36)$$

the terms can be expanded over electron index

$$E_{ee} = \frac{1}{2} \left[ \iint \frac{1}{|\vec{r}_1 - \vec{r}_2|} d\vec{r}_1 d\vec{r}_2 \int |\psi(\vec{r}_1, \dots, \vec{r}_N)|^2 d\vec{r}_3 d\vec{r}_4 \dots d\vec{r}_N + \iint \frac{1}{|\vec{r}_1 - \vec{r}_3|} d\vec{r}_1 d\vec{r}_3 \int |\psi(\vec{r}_1, \dots, \vec{r}_N)|^2 d\vec{r}_2 d\vec{r}_4 \dots d\vec{r}_N + \dots \right] \quad (2.37)$$

The second integral at each term is similar to the definition of density. Using same consideration which is used when writing the nucleus electron interaction the electron electron energy can be written as

$$E_{ee} = \frac{1}{2} \frac{1}{N_e^2} \left[ \iint \frac{n(\vec{r}_1, \vec{r}_2)}{|\vec{r}_1 - \vec{r}_2|} d\vec{r}_1 d\vec{r}_2 + \iint \frac{n(\vec{r}_1, \vec{r}_3)}{|\vec{r}_1 - \vec{r}_3|} d\vec{r}_1 d\vec{r}_3 + \dots \right] \quad (2.38)$$

Again the variables in the definition of density can be replaced by dummy indices so this equation becomes

$$E_{ee} = \frac{1}{2} \left[ \iint \frac{n(\vec{r}, \vec{r}')}{|\vec{r} - \vec{r}'|} d\vec{r} d\vec{r}' \right] \quad (2.39)$$

Here  $n(\vec{r}, \vec{r}')$  means the probability of being one electron at point  $\vec{r}$  and the other being at  $\vec{r}'$ . Because of this term the many body problem is hard to solve. In addition to this, DFT does not support two particle density, so this term should be approximated considering two electrons are uncorrelated.

$$n(\vec{r}, \vec{r}') = n(\vec{r})n(\vec{r}') + \Delta n(\vec{r}, \vec{r}') \quad (2.40)$$

Two particle density is written as product of one particle densities plus a correction. Considering this approximation, the electron electron energy can be written with a correction term.

$$E_{ee} = \frac{1}{2} \iint \frac{n(\vec{r})n(\vec{r}')}{|\vec{r} - \vec{r}'|} d\vec{r} d\vec{r}' + \Delta E_{ee} \quad (2.41)$$

When all terms are put together, the ground state electronic energy can be written as

$$E_e = -\frac{1}{2} \sum_n^{N_e} \int d\vec{r} \phi_n^*(\vec{r}) \nabla^2 \phi_n(\vec{r}) + \int n(\vec{r}) V_{ne}(\vec{r}) d\vec{r} + \frac{1}{2} \iint \frac{n(\vec{r})n(\vec{r}')}{|\vec{r} - \vec{r}'|} d\vec{r} d\vec{r}' + \Delta E_{ee} + \Delta T \quad (2.42)$$

The last two terms can be collected under one term which is called the exchange-correlation term.

$$E_{xc} = \Delta E_{ee} + \Delta T \quad (2.43)$$

### 2.3 THE HOHENBERG-KOHN THEOREMS

The Hohenberg-Kohn theorems are the most important theorems for DFT because they make it possible. The first Hohenberg-Kohn theorem states that if the ground state electron density of a system is known, then any ground state property can be found [17]. It is assumed that there are  $N$  electrons in the system which move under influence of an external potential. The Hamiltonian of this system can be written as Eq. 2.20, considering the effect of nucleus on

electrons as external potential

$$-\sum_I \sum_i^{Nn} \frac{Z_I}{|\vec{r}_i - \vec{R}_I|} = \sum_{i=1}^N V_{ext}(\vec{r}_i) \quad (2.44)$$

due to simplify the last term of equation 2.20, it can be written as

$$\frac{1}{2} \sum_i^{Ne} \sum_{j \neq i}^{Ne} \frac{1}{|\vec{r}_i - \vec{r}_j|} = V(\vec{r}_1, \vec{r}_2, \dots, \vec{r}_N) \quad (2.45)$$

Then the Hamiltonian of N electron system which moves under influence of external potential is

$$\hat{H} = -\frac{1}{2} \sum_i^N \nabla_i^2 + \sum_{i=1}^N V_{ext}(\vec{r}_i) + V(\vec{r}_1, \vec{r}_2, \dots, \vec{r}_N) \quad (2.46)$$

It is assumed that there are two different potentials  $V_{ext,1}$  and  $V_{ext,2}$  acting on the same system separately, so there should be two different hamiltonian. It is also assumed that these two potentials are differed by more than a constant.

$$\hat{H}_1 = -\frac{1}{2} \sum_i^N \nabla_i^2 + \sum_{i=1}^N V_{ext,1}(\vec{r}_i) + V(\vec{r}_1, \vec{r}_2, \dots, \vec{r}_N) \quad (2.47a)$$

$$\hat{H}_2 = -\frac{1}{2} \sum_i^N \nabla_i^2 + \sum_{i=1}^N V_{ext,2}(\vec{r}_i) + V(\vec{r}_1, \vec{r}_2, \dots, \vec{r}_N) \quad (2.47b)$$

Also there should be two different wavefunctions for the ground states  $\psi_1$  and  $\psi_2$ .

$$\hat{H}_1 \psi_1 = E_1 \psi_1 \quad (2.48a)$$

$$\hat{H}_2 \psi_2 = E_2 \psi_2 \quad (2.48b)$$

Here  $\psi_1 \neq \psi_2$ . However, the basic assumption is that  $\psi_1$  and  $\psi_2$  give the same density.

$$n(\vec{r}) = \langle \psi_1 | \hat{n}(\vec{r}) | \psi_1 \rangle = \langle \psi_2 | \hat{n}(\vec{r}) | \psi_2 \rangle \quad (2.49)$$

Then the variational principle says that there is no wavefunction  $\psi$  which can give less energy than the ground state wavefunction of each Hamiltonian.

$$\langle \psi_1 | \hat{H}_1 | \psi_1 \rangle = E_1 < \langle \psi | \hat{H}_1 | \psi \rangle \quad (2.50)$$

The random wavefunction can be chosen as  $\psi_2$ ,

$$\langle \psi_2 | \hat{H}_1 | \psi_2 \rangle > E_1 \quad (2.51)$$

$\hat{H}_2$  can be added to and subtracted from the first term of 2.51. Then, using Eq. 2.47 and the definition of density Eq. 2.51 can be written as

$$E_1 - E_2 < \int n(\vec{r}) [V_{ext,1}(\vec{r}) - V_{ext,2}(\vec{r})] d\vec{r} \quad (2.52)$$

The same procedure can be used in the case of changing  $\psi_1$  with  $\psi_2$

$$E_2 - E_1 < \int n(\vec{r}) [V_{ext,2}(\vec{r}) - V_{ext,1}(\vec{r})] d\vec{r} \quad (2.53)$$

The equations 2.52 and 2.53 are in a contradiction. These two equations can not be true simultaneously. This means that the basic assumption;  $\psi_1$  and  $\psi_2$  give the same density, is not correct. The conclusion of first Hohenberg-Kohn theorem is that two different external potentials can not produce the same electron density [15]. The density is uniquely determined for the external potential. Thus, the ground state properties of interacting particles system can be uniquely defined by only knowing the electron density.

The second Hohenberg-Kohn theorem is based on variational principle. It is considered that the treatment of kinetic energy and the internal potential energy is the same for all systems. Thus, these two energies can be assigned to universal functional  $F[n]$ . Then the electronic energy can be written as

$$E_e[n] = F[n] + \int V_{ext}(\vec{r})n(\vec{r}) \quad (2.54)$$

This energy is equal to the ground state energy if  $n(\vec{r})$  is the ground state electron density and  $\psi$  is the ground state wavefunction. Thus, the ground state electronic energy can be written as

$$E_e[n] = \min_{\psi \rightarrow n} \langle \psi | \hat{H}_e | \psi \rangle \quad (2.55)$$

Then a different density  $n'(\vec{r})$  can be used instead of  $n(\vec{r})$ . Since the densities are different, they can not be constructed from same wavefunctions. Using the new density the electronic energy is

$$E_e[n'] = \min_{\psi' \rightarrow n'} \langle \psi' | \hat{H}_e | \psi' \rangle \quad (2.56)$$

The new wavefunction can not be the ground state of the system so the expectation value electronic Hamiltonian should give a higher energy than the exact ground state energy.

$$E_e[n'] > E_e[n] \quad (2.57)$$

The conclusion of second Hohenberg-Kohn theorem is that the electronic energy can be written in terms of density and the correct density that minimizes the electronic energy is then ground state density. If the universal functional  $F[n]$  is known and it is simple then determining ground state energy and density will be easier. Throught the proof of each Hohenberg-Kohn theorems it is considered that the energy levels are non-degenerate. If they are degenerate, then the first theorem can not be proven.

## 2.4 KOHN-SHAM EQUATIONS

Practical usage of Hohenberg-Kohn theorems are provided by Kohn and Sham [18]. The second Hohenberg-Kohn theorem states that for the exact ground state density the electronic energy  $E_e[n]$  will be minimum. Thus, change in density do not make any variation to the ground state energy

$$\delta E_e[n] \equiv E_e[n + \delta n] - E_e[n] = 0 \quad (2.58)$$

assuming the change in  $n$  do not change the total number of electrons. Then using Lagrange multipliers method this equation can be written as

$$\delta[E_e[n(\vec{r})] - \sum_{i,j} \lambda_{i,j}(\langle \phi_i | \phi_j \rangle - \delta_{ij})] = 0 \quad (2.59)$$

Using the properties of functional derivatives this equation becomes

$$\frac{\delta}{\delta \phi_i^*(\vec{r})} [E_e[n(\vec{r})] - \sum_{i,j} \lambda_{i,j}(\langle \phi_i | \phi_j \rangle - \delta_{ij})] = 0 \quad (2.60)$$

The main idea was minimization of total energy with respect to density but kinetic energy term can not be written in terms of density so it is preferred to perform the minimization with respect to complex conjugate of orbitals instead of density. As it was stated before both of them give the same result, then this equation can be written

$$\begin{aligned} \frac{\delta}{\delta \phi_i^*(\vec{r})} \left[ -\frac{1}{2} \sum_n^{N_e} \int d\vec{r} \phi_n^*(\vec{r}) \nabla^2 \phi_n(\vec{r}) \right] + \frac{\delta}{\delta n(\vec{r})} \left[ \int n(\vec{r}) V_{ne}(\vec{r}) d\vec{r} + \right. \\ \left. \frac{1}{2} \iint \frac{n(\vec{r})n(\vec{r}')}{|\vec{r} - \vec{r}'|} d\vec{r} d\vec{r}' + \int d\vec{r} n(\vec{r}) \epsilon_{xc}(n(\vec{r})) \right] \frac{\delta n(\vec{r})}{\delta \phi_i^*(\vec{r})} = \epsilon_i \phi_i(\vec{r}) \end{aligned} \quad (2.61)$$

Again using the properties of functional derivative and considering  $\epsilon_{xc}(n(\vec{r}))$  is also a functional of  $n(\vec{r})$  Eq. 2.61 becomes,

$$-\frac{1}{2} \nabla^2 \phi_i(\vec{r}) + \left[ V_{ne}(\vec{r}) + \int \frac{n(\vec{r}')}{|\vec{r} - \vec{r}'|} d\vec{r}' + \epsilon_{xc}[n(\vec{r})] + n(\vec{r}) \frac{\delta \epsilon_{xc}[n(\vec{r})]}{\delta n(\vec{r})} \right] \phi_i(\vec{r}) = \epsilon_i \phi_i(\vec{r}) \quad (2.62)$$

In fact equation 2.62 is a set of equations. If they are solved simultaneously, they represent the many-particle system in terms of single particle orbitals. Second term in the parenthesis is called Hartree potential, the third and the final terms are called exchange correlation potential. All the terms in the parenthesis can be assigned to  $V_{eff}$ . Then each equation becomes Schrödinger like equations.

$$[\hat{T} + V_{eff}] \phi(\vec{r}) = \epsilon_i \phi_i(\vec{r}) \quad (2.63)$$

This set of equation is called Kohn-Sham equations. The trick of Kohn-Sham equations is that instead of the real many particle system, a fictitious system of non-interacting particles which has the same energy and density as the real system is considered and these non-interacting particles move under external potential  $V_{eff}$  [15]. The difference between each Kohn-Sham equation and Schrödinger equation is that the  $V_{eff}$  directly depends on density and indirectly depends on orbitals. This situation is a little unusual because if there is a change in orbitals then the potential which depends on orbitals will also change so, Kohn-Sham set of equations should be solved self-consistently. The eigenvalues of Kohn-Sham equations do not have a significance since considering the interacting many particle system as a collection of noninteracting single-particle systems is not correct. However, the Kohn-Sham orbitals give quite accurate results for description of band structures and bonding characters.

## 2.5 PLANEWAVE EXPANSION

In order to solve Kohn-Sham equations easily, it should be expanded in terms of suitable basis, for example planewave basis. Then, it should be converted to matrix equation in reciprocal (momentum,coefficient) space.

### 2.5.1 Reciprocal space

The solids are actually finite systems with bounding surfaces. However, they are considered as infinite systems for practical purposes. This consideration imposes periodicity in all three dimensions for the wavefunction.

$$\psi(\vec{r}) = \psi(\vec{r} + N_1\vec{a}_1) = \psi(\vec{r} + N_2\vec{a}_2) = \psi(\vec{r} + N_3\vec{a}_3) \quad (2.64)$$

These boundary conditions are called Born-von Karman boundary conditions. These boundary conditions imply that the physical properties such as charge density and magnetic moment density, are invariant under  $\hat{T}(n_1, n_2, n_3)$  for crystals [19].

$$f(\vec{r} + \hat{T}(n_1, n_2, n_3)) = f(\vec{r}) \quad (2.65)$$

where  $\hat{T}(n_1, n_2, n_3) = n_1\vec{a}_1 + n_2\vec{a}_2 + n_3\vec{a}_3$  and  $a_i, i = 1, 2, 3$  are primitive translational vectors. The Fourier components of those periodic functions are easier to handle than real space components under same circumstances. The forward Fourier component of any periodic function,

using  $q$  as a wavevector defined in reciprocal space as;

$$f(\vec{q}) = \frac{1}{\Omega_{crystal}} \int_{\Omega_{crystal}} d\vec{r} f(\vec{r}) e^{-i\vec{q} \cdot \vec{r}} \quad (2.66)$$

Each component of the periodic function should satisfy Born-Von Karmen boundary conditions. If a translation vector  $T(n_1, n_2, n_3)$  is added to  $\vec{r}$  the Fourier component of periodic function will still be the same.

$$\begin{aligned} f(\vec{q}) &= \frac{1}{\Omega_{crystal}} \sum_{n_1, n_2, n_3} \int_{\Omega_{crystal}} d\vec{r} f(\vec{r}) e^{-i\vec{q} \cdot (\vec{r} + T(n_1, n_2, n_3))} \\ &= \frac{1}{N_{cell}} \sum_{n_1, n_2, n_3} e^{-iq \cdot T(n_1, n_2, n_3)} \frac{1}{\Omega_{cell}} \int_{\Omega_{cell}} d\vec{r} f(\vec{r}) e^{-i\vec{q} \cdot \vec{r}} \\ &= \frac{1}{N_{cell}} \prod_i \sum_{n_i} e^{-i(q \cdot \vec{a}_i)^{n_i}} \frac{1}{\Omega_{cell}} \int_{\Omega_{cell}} d\vec{r} f(\vec{r}) e^{-i\vec{q} \cdot \vec{r}} \end{aligned} \quad (2.67)$$

This equation is written using the property in equation 2.65. Equations 2.66 and 2.67 should be equal to each other. This concludes that

$$e^{i\vec{q} \cdot \vec{a}_i)^{n_i}} = 1 \quad (2.68)$$

Equation 2.68 yields a restriction and a quantization rule on the wavevector  $\vec{q}$ .

$$\vec{q} \cdot \vec{a}_i = 2\pi m \quad (2.69)$$

where  $m$  is an integer. The set of  $q$ 's that satisfy the condition in equation 2.69 create reciprocal lattice. The minimal set of  $q$  vectors which can span all the reciprocal space can be defined as  $b_i$ ,  $i = 1, 2, 3$  and the relation to the space lattice vectors is that

$$\vec{b}_i \cdot \vec{a}_j = 2\pi \delta_{ij} \quad (2.70)$$

Any point on the reciprocal space can be defined by

$$\vec{G}(m_1, m_2, m_3) = m_1 \vec{b}_1 + m_2 \vec{b}_2 + m_3 \vec{b}_3 \quad (2.71)$$

where the reciprocal space vectors  $b_i$ 's can be written in terms of real space vectors as

$$\vec{b}_i = 2\pi \frac{\vec{a}_j \times \vec{a}_k}{\vec{a}_i \cdot (\vec{a}_j \times \vec{a}_k)} \quad (2.72)$$

Then the Fourier transform of periodic function is written

$$f(\vec{G}) = \frac{1}{\Omega_{crystal}} \int_{\Omega_{crystal}} d\vec{r} f(\vec{r}) e^{-i\vec{G} \cdot \vec{r}} \quad (2.73)$$

## 2.5.2 Bloch's theorem

Similar to the periodic functions, the Hamiltonian operator is also invariant under lattice translation. This means that the Hamiltonian commutes with the translation operator.

$$[\hat{H}, \hat{T}_{\vec{n}}] = 0 \quad (2.74)$$

The translation operator can be defined as

$$\hat{T}_{\vec{n}} = \vec{n}_1 \vec{d}_1 + \vec{n}_2 \vec{d}_2 + \vec{n}_3 \vec{d}_3 \quad (2.75)$$

It is known that if two operators commutes with each other, they have common eigenfunctions

$$\begin{aligned} \hat{H}\psi(\vec{r}) &= \epsilon\psi(\vec{r}) \\ \hat{T}_{\vec{n}}\psi(\vec{r}) &= t_{\vec{n}}\psi(\vec{r}) \end{aligned} \quad (2.76)$$

where  $t_{\vec{n}}$  is the eigenvalue of translation operator. If this operator acts on the eigenfunction  $N$  times, according to the Born-Von Karman boundary conditions, the eigenfunction will remain unchanged.

$$\hat{T}_{\vec{n}}^N \psi(\vec{r}) = (t_{\vec{n}})^N \psi(\vec{r}) = \psi(\vec{r}) \quad (2.77)$$

This equation leads to

$$(t_{\vec{n}})^N = 1 \quad (2.78)$$

Then the eigenvalue of translation operator can be written as

$$t_{\vec{n}} = e^{ik \cdot \hat{T}_{\vec{n}}} \quad (2.79)$$

using Eq. 2.79 the equation 2.77 becomes

$$\hat{T}_{\vec{n}} \psi(\vec{r}) = e^{ik \cdot \hat{T}_{\vec{n}}} \psi(\vec{r}) \quad (2.80)$$

where

$$\vec{k} = \frac{n_1}{N} b_1 + \frac{n_2}{N} b_2 + \frac{n_3}{N} b_3 \quad (2.81)$$

Equation 2.79 is the Bloch's Theorem and it says that the lattice periodic Hamiltonian's wavefunction takes a phase factor when translational operator acts on it. Here  $\vec{k}$  is a reciprocal space vector and it is restricted to the first Brillouin zone which is the primitive cell of the lattice in reciprocal space. In Bloch's formalism the wavefunction in equation 2.80 can be written as

$$\psi(\vec{r}) = e^{i\vec{k} \cdot \vec{r}} u_{\vec{k}}(\vec{r}) \quad (2.82)$$

$u_{\vec{k}}(\vec{r})$  is lattice periodic function which has the three-dimensional periodicity of the crystal lattice

$$u_{\vec{k}}(\vec{r} + \vec{T}_n) = u_{\vec{k}}(\vec{r}) \quad (2.83)$$

By using Bloch theorem, the wavefunction of the system is divided into lattice periodic function and a phase factor on it. Then the Schrödinger equation can be written in terms of Bloch wavefunctions given in Eq. 2.82.

$$\begin{aligned} \hat{H}\psi_{i,\vec{k}}(\vec{r}) &= \epsilon_{i,\vec{k}}(\vec{r})\psi_{i,\vec{k}}(\vec{r}) \\ \hat{H}e^{i\vec{k}\cdot\vec{r}}u_{i,\vec{k}}(\vec{r}) &= \epsilon_{i,\vec{k}}(\vec{r})e^{i\vec{k}\cdot\vec{r}}u_{i,\vec{k}}(\vec{r}) \end{aligned} \quad (2.84)$$

If Eq. 2.84 is multiplied by complex conjugate of the phase factor,

$$\begin{aligned} e^{-i\vec{k}\cdot\vec{r}}\hat{H}e^{i\vec{k}\cdot\vec{r}}u_{i,\vec{k}}(\vec{r}) &= \epsilon_{i,\vec{k}}(\vec{r})u_{i,\vec{k}}(\vec{r}) \\ \hat{H}_{\vec{k}}u_{i,\vec{k}}(\vec{r}) &= \epsilon_{i,\vec{k}}(\vec{r})u_{i,\vec{k}}(\vec{r}) \end{aligned} \quad (2.85)$$

Where  $\hat{H}_{\vec{k}}$  is wavevector dependent Hamiltonian. If the new Hamiltonian is solved for each wavevector inside the Brillouin zone, a spectrum of eigenvalues for each wavevector will be observed. This spectrum is very important for analyzing electronic properties of the crystal and is called the band structure.

The Kohn-Sham equations can be handled easier when it is converted to the matrix equation in coefficient space. The Kohn-Sham orbitals should be converted to the reciprocal space using plane waves as a basis set. The plane wave basis have some advantage over the other basis sets such as atomic wavefunctions. Plane waves are mathematically simple functions and they form complete a set in Hilbert space. Moreover, they cover the space equally. However, when the system has nonuniform electron density, this property is no longer an advantage.

$$\begin{aligned} [\hat{T} + V_{eff}]\phi(\vec{r}) &= \epsilon_i\phi_i(\vec{r}) \\ \hat{H}_{eff}\phi(\vec{r}) &= \epsilon_i\phi_i(\vec{r}) \end{aligned} \quad (2.86)$$

The Kohn-Sham orbitals can be expanded in terms of planewaves as

$$\phi_i(\vec{r}) = \sum_{\vec{q}} c_{i,\vec{q}} \frac{1}{\sqrt{\Omega}} e^{i\vec{q}\cdot\vec{r}} \quad (2.87)$$

in Bra-Ket notation

$$\phi_i(\vec{r}) = \sum_{\vec{q}} c_{i,\vec{q}} |\vec{q}\rangle \quad (2.88)$$

The inner product of planewaves

$$\langle \vec{q}' | \vec{q} \rangle = \frac{1}{\Omega} \int_{\Omega} d\vec{r} e^{-i\vec{q}'\cdot\vec{r}} e^{i\vec{q}\cdot\vec{r}} = \delta_{\vec{q},\vec{q}'} \quad (2.89)$$

The Kohn-Sham equation can be converted to matrix equation in coefficient space by multiplying the equation 2.86 with  $\langle \vec{q}' |$  and integrating in real space.

$$\sum_{\vec{q}} \langle \vec{q}' | \hat{H}_{eff} | \vec{q} \rangle c_{i,\vec{q}} = \epsilon_i \sum_{\vec{q}} \langle \vec{q}' | \vec{q} \rangle c_{i,\vec{q}} = \epsilon_i c_{i,\vec{q}} \quad (2.90)$$

This is the matrix equation and it can be written simply as

$$\bar{H}C = \epsilon_i C \quad (2.91)$$

For the general  $\vec{q} = \vec{k} + \vec{G}_m$  and  $\vec{q}' = \vec{k} + \vec{G}_{m'}$  can be used. The terms in Kohn-Sham equations can be converted term by term. The first term is the kinetic energy term which has diagonal form

$$\langle \vec{k} + \vec{G}_{m'} | -\frac{1}{2} \nabla^2 | \vec{k} + \vec{G}_m \rangle = -\frac{1}{2} |\vec{k} + \vec{G}_m|^2 \delta_{\vec{k} + \vec{G}_{m'}, \vec{k} + \vec{G}_m} \quad (2.92)$$

The potential part can be converted using Fourier transform.

$$V_{eff}(\vec{r}) = \sum_m V_{eff}(\vec{G}_m) e^{i\vec{G}_m \cdot \vec{r}} \quad (2.93)$$

This can be converted to a matrix equation as

$$\langle \vec{k} + \vec{G}_{m'} | V_{eff} | \vec{k} + \vec{G}_m \rangle = \sum_m \langle \vec{k} + \vec{G}_{m'} | V_{eff}(\vec{G}_m) | \vec{k} + \vec{G}_m \rangle e^{i\vec{G}_m \cdot \vec{r}} \quad (2.94)$$

The ket  $|\vec{k} + \vec{G}_m\rangle$  is equal to  $e^{i(\vec{k} + \vec{G}_m) \cdot \vec{r}}$  then this equation can be written as

$$\begin{aligned} \langle \vec{k} + \vec{G}_{m'} | V_{eff} | \vec{k} + \vec{G}_m \rangle &= \sum_m V_{eff}(\vec{G}_m) \langle \vec{k} + \vec{G}_{m'} | \vec{k} + 2\vec{G}_m \rangle \\ &= \sum_m V_{eff}(\vec{G}_m) \langle \vec{G}_{m'} - \vec{G}_m | \vec{G}_m \rangle \end{aligned} \quad (2.95)$$

For a specific  $\vec{k}$ , the sum over  $\vec{q}$  in equation 2.90 can be converted to sum over  $m$ .

$$\sum_m \langle \vec{k} + \vec{G}_{m'} | \hat{H}_{eff} | \vec{k} + \vec{G}_m \rangle c_{i,m} = \epsilon_i c_{i,m'} \quad (2.96)$$

Similar to equation 2.85 in Bloch theorem this equation can be written with  $\vec{k}$ -dependence.

$$\sum_m H_{m',m}(\vec{k}) c_{i,m}(\vec{k}) = \epsilon_i(\vec{k}) c_{i,m'}(\vec{k}) \quad (2.97)$$

where  $H_{m',m}(\vec{k}) = \frac{1}{2} |\vec{k} + \vec{G}_m|^2 \delta_{m',m} + V_{eff}(\vec{G}_m - \vec{G}_{m'})$  using equation 2.92 and 2.95.

### 2.5.3 $V_{eff}$ in Terms of Planewaves

The  $V_{eff}(\vec{G}_m - \vec{G}_{m'})$  includes external potential term, Hartree potential term and exchange correlation potential term as it can be seen in equation 2.62, so these terms should be written in terms of planewaves in reciprocal space also.

### 2.5.3.1 Hartree potential term in terms of planewaves

The Hartree potential term was

$$V_H(\vec{r}) = \int d\vec{r}' \frac{n(\vec{r}')}{|\vec{r} - \vec{r}'|} \quad (2.98)$$

Using equation 2.73 the fourier component of hartree potential term can be written as

$$\begin{aligned} V_H(\vec{G}) &= \frac{1}{\Omega_{crystal}} \int_{\Omega_{crystal}} d\vec{r} V_H(\vec{r}) e^{-i\vec{G}\cdot\vec{r}} \\ &= \frac{1}{\Omega_{crystal}} \int_{\Omega_{crystal}} \int d\vec{r} d\vec{r}' \frac{n(\vec{r}')}{|\vec{r} - \vec{r}'|} e^{-i\vec{G}\cdot\vec{r}} \end{aligned} \quad (2.99)$$

using the identity

$$n(\vec{r}) = \sum_{\vec{G}} n(\vec{G}) e^{-i\vec{G}\cdot\vec{r}} \quad (2.100)$$

equation 2.108 can be written as

$$V_H(\vec{G}) = \frac{1}{\Omega_{crystal}} \sum_{\vec{G}'} \int_{\Omega_{crystal}} \int d\vec{r} d\vec{r}' \frac{n(\vec{G}')}{|\vec{r} - \vec{r}'|} e^{-i\vec{G}'\cdot\vec{r}'} e^{-i\vec{G}\cdot\vec{r}} \quad (2.101)$$

make change of variable  $\vec{u} = \vec{r} - \vec{r}'$

$$V_H(\vec{G}) = \frac{1}{\Omega_{crystal}} \sum_{\vec{G}'} n(\vec{G}') \int_{\Omega_{crystal}} d\vec{r}' e^{-i(\vec{G}+\vec{G}')\cdot\vec{r}'} \int d\vec{u} e^{-i\vec{G}\cdot\vec{u}} \quad (2.102)$$

The first integral gives the Kronecker delta and the second integral can be calculating using volume integral

$$V_H(\vec{G}) = \frac{1}{\Omega_{crystal}} \sum_{\vec{G}'} n(\vec{G}') \Omega_{cell} \delta_{\vec{G}, \vec{G}'} \int_0^{2\pi} \phi \int_0^\infty \int_{-1}^1 u^2 du (-d\cos\theta) \frac{e^{-iG u \cos\theta}}{u} \quad (2.103)$$

using the Kronecker delta and taking the  $d\cos\theta$  integral

$$V_H(\vec{G}) = 2\pi n(\vec{G}) \int \frac{e^{iGu} - e^{-iGu}}{-iG} du \quad (2.104)$$

This integral cen be calculated using regulator  $u = u + i\mu$ .

$$V_H(\vec{G}) = 2\pi n(\vec{G}) \lim_{\mu \rightarrow 0} \frac{e^{iG(u+i\mu)} - e^{-iG(u+i\mu)}}{G^2} \quad (2.105)$$

When the limit when  $\mu \rightarrow 0$  is taken, Fourier representation of the Hartree potential can be written as

$$V_H(\vec{G}) = 4\pi \frac{n(\vec{G})}{G^2} \quad (2.106)$$

### 2.5.3.2 Exchange correlation potential term in terms of planewaves

The exchange correlation potential was

$$V_{xc} = \epsilon_{xc}[n(\vec{r})] + n(\vec{r}) \frac{\delta \epsilon_{xc}[n(\vec{r})]}{\delta n(\vec{r})} \quad (2.107)$$

again using 2.73 the Fourier component of exchange correlation potential can be written as

$$\begin{aligned} V_{xc}(\vec{G}) &= \frac{1}{\Omega_{crystal}} \int_{\Omega_{crystal}} d\vec{r} V_{xc}(\vec{r}) e^{-i\vec{G}\cdot\vec{r}} \\ &= \frac{1}{\Omega_{crystal}} \int_{\Omega_{crystal}} d\vec{r} \left( \epsilon_{xc}[n(\vec{r})] + n(\vec{r}) \frac{\delta \epsilon_{xc}[n(\vec{r})]}{\delta n(\vec{r})} \right) e^{-i\vec{G}\cdot\vec{r}} \end{aligned} \quad (2.108)$$

This equation can be separated

$$V_{xc}(\vec{G}) = \frac{1}{\Omega_{crystal}} \int_{\Omega_{crystal}} d\vec{r} \epsilon_{xc}[n(\vec{r})] e^{-i\vec{G}\cdot\vec{r}} + \frac{1}{\Omega_{crystal}} \int_{\Omega_{crystal}} d\vec{r} n(\vec{r}) \frac{\delta \epsilon_{xc}[n(\vec{r})]}{\delta n(\vec{r})} e^{-i\vec{G}\cdot\vec{r}} \quad (2.109)$$

The first term is look like the Fourier component of  $\epsilon[\vec{r}]$  and the identity in equation 2.100 can be used;

$$V_{xc}(\vec{G}) = \epsilon_{xc}(\vec{G}) + \frac{1}{\Omega_{crystal}} \int_{\Omega_{crystal}} d\vec{r} \sum_{\vec{G}', \vec{G}''} n(\vec{G}'') e^{-i\vec{G}''\cdot\vec{r}} \frac{\delta \epsilon_{xc}(\vec{G}')}{\delta n(\vec{G}')} e^{-i\vec{G}'\cdot\vec{r}} e^{-i\vec{G}\cdot\vec{r}} \quad (2.110)$$

then the exponential term is put to together

$$V_{xc}(\vec{G}) = \epsilon_{xc}(\vec{G}) + \sum_{\vec{G}', \vec{G}''} n(\vec{G}'') \frac{\delta \epsilon_{xc}(\vec{G}')}{\delta n(\vec{G}')} \frac{1}{\Omega_{crystal}} \int_{\Omega_{crystal}} e^{-i(\vec{G} + \vec{G}' + \vec{G}'')\cdot\vec{r}} d\vec{r} \quad (2.111)$$

using the property of Kronecker delta. This equation can be written as

$$V_{xc}(\vec{G}) = \epsilon_{xc}(\vec{G}) + \sum_{\vec{G}} n_{xc}(\vec{G} - \vec{G}') \frac{d\epsilon_{xc}}{dn}(\vec{G}') \quad (2.112)$$

### 2.5.3.3 External potential term in terms of planewaves

Consider a system which contains  $n_{sp}$  different species of atoms each species having  $n^k$  identical atoms at  $\vec{r}_{\kappa,j}$ . Then the external potential can be written as the sum of these components

$$V_{ext}(\vec{r}) = \sum_{\kappa} \sum_{j=1}^{n_{sp}} \sum_{\vec{r}} V^{\kappa}(\vec{r} - \vec{r}_{\kappa,j} - \vec{T}) \quad (2.113)$$

using equation 2.73 Fourier component of this term can be written as

$$\begin{aligned} V_{ext}(\vec{G}) &= \frac{1}{\Omega_{crystal}} \int_{\Omega_{crystal}} d\vec{r} V_{ext}(\vec{r}) e^{-i\vec{G}\cdot\vec{r}} \\ &= \frac{1}{\Omega_{crystal}} \int_{\Omega_{crystal}} d\vec{r} \sum_{\kappa} \sum_{j=1}^{n_{sp}} \sum_{\vec{r}} V^{\kappa}(\vec{r} - \vec{r}_{\kappa,j} - \vec{T}) e^{-i\vec{G}\cdot\vec{r}} \end{aligned} \quad (2.114)$$

make change of variable  $\vec{u} = \vec{r} - \vec{\tau}_{\kappa,j} - \vec{T}$

$$V_{ext}(\vec{G}) = \frac{1}{\Omega_{crystal}} \sum_{\kappa} \sum_{j=1}^{n_{sp}} \sum_{\vec{T}} \int_{\Omega_{crystal}} d\vec{u} V^{\kappa}(\vec{u}) e^{-i\vec{G} \cdot (\vec{u} + \vec{\tau}_{\kappa,j} + \vec{T})} \quad (2.115)$$

using the formulas

$$\sum_{n=0}^{N-1} e^{inx} = \frac{1 - e^{iNx}}{1 - e^{ix}} \quad (2.116)$$

$$e^x = \sum_{n=0}^{\infty} \frac{x^n}{n!}$$

Equation 2.115 can be written as

$$V_{ext}(\vec{G}) = \frac{1}{\Omega_{crystal}} \sum_{\kappa} \sum_{j=1}^{n_{sp}} \int_{\Omega_{crystal}} d\vec{u} V^{\kappa}(\vec{u}) e^{-i\vec{G} \cdot (\vec{u} + \vec{\tau}_{\kappa,j})} \sum_{\vec{T}} e^{-i\vec{G} \cdot \vec{T}} \quad (2.117)$$

$$= \frac{1}{\Omega_{crystal}} \sum_{\kappa} \sum_{j=1}^{n_{sp}} \int_{\Omega_{crystal}} d\vec{u} V^{\kappa}(\vec{u}) e^{-i\vec{G} \cdot (\vec{u} + \vec{\tau}_{\kappa,j})} N_{cell}$$

The exponential can also be separated and the relation  $\Omega_{crystal} = N_{cell} \Omega_{cell}$  is known

$$V_{ext}(\vec{G}) = \frac{1}{\Omega_{cell}} \sum_{\kappa} \int_{\Omega} d\vec{u} V^{\kappa}(\vec{u}) e^{-i\vec{G} \cdot \vec{u}} \sum_{j=1}^{n_{sp}} e^{-i\vec{G} \cdot \vec{\tau}_{\kappa,j}} \quad (2.118)$$

The integral is equal to  $V^{\kappa}(\vec{G}) \Omega_{\kappa}$  using equation 2.73

$$V_{ext}(\vec{G}) = \sum_{\kappa} \frac{\Omega_{\kappa}}{\Omega_{cell}} V^{\kappa}(\vec{G}) \sum_{j=1}^{n_{sp}} e^{-i\vec{G} \cdot \vec{\tau}_{\kappa,j}} \quad (2.119)$$

The second sum is called structure factor  $S^{\kappa}(\vec{G})$

$$V_{ext}(\vec{G}) = \sum_{\kappa} \frac{\Omega_{\kappa}}{\Omega_{cell}} V^{\kappa}(\vec{G}) S^{\kappa}(\vec{G}) \quad (2.120)$$

this implies that the Fourier component of external potential is divided to Fourier component of the isolated atomic potential and the sum of planewaves which is the periodic part.

## 2.5.4 Density in terms of planewaves

The electron density in real space is written

$$n(\vec{r}) = \sum_n^{N_e} |\phi_n(\vec{r})|^2 \quad (2.121)$$

and the planewave is

$$\phi_i(\vec{r}) = \frac{1}{\sqrt{\Omega}} \sum_{\vec{k}} c_{i,\vec{k}} e^{i\vec{k}\cdot\vec{r}} \quad (2.122)$$

put this in equation 2.121 and impose the  $k$  dependence to the density

$$n_{i,\vec{k}}(\vec{G}) = \frac{1}{\Omega} \sum_m c_{i,m}^*(\vec{k}) c_{i,m''}(\vec{k}) \quad (2.123)$$

All the terms in the Eq. 2.123 are written in terms of planewaves but the complete expansion of planewaves can not be considered. Thus, in DFT codes the planewaves are cut off by giving a parameter to the code. The code takes the planewaves which satisfy

$$\frac{1}{2}|\vec{G}|^2 < E_{cut} \quad (2.124)$$

This cut off parameter is defined by performing a convergence study [20].

## 2.6 EXCHANGE and CORRELATION ENERGY FUNCTIONALS

The crucial point in density functional theory is exchange-correlation energy functional. Basically there are two different functionals in literature, the local density approximation (LDA) and generalized gradient approximation (GGA).

### 2.6.1 The Local density approximation

In LDA [17], exchange-correlation energy is equal to the integral of exchange-correlation energy density which is taken to be the same with homogeneous electron gas having same density. More generally LDA is called local spin density approximation (LSDA) [15]

$$\begin{aligned} E_{xc}^{LSDA}[n^\uparrow, n^\downarrow] &= \int d^3r n \vec{r} \epsilon_{xc}^{hom}(n^\uparrow(\vec{r}), n^\downarrow(\vec{r})) \\ &= \int d^3r n \vec{r} [\epsilon_x^{hom}(n^\uparrow(\vec{r}), n^\downarrow(\vec{r})) + \epsilon_c^{hom}(n^\uparrow(\vec{r}), n^\downarrow(\vec{r}))] \end{aligned} \quad (2.125)$$

The exchange and the correlation terms can be separated linearly. LSDA can be formulated using spin up densities  $n^\uparrow(\vec{r})$  and spin down densities  $n^\downarrow(\vec{r})$  or it can be formulated using the total density  $n(\vec{r})$  which is called LDA in that case. The fractional spin polarization is that

$$\xi(\vec{r}) = \frac{n^\uparrow(\vec{r}) - n^\downarrow(\vec{r})}{n(\vec{r})} \quad (2.126)$$

It is assumed that the  $E_{xc}[n^\uparrow, n^\downarrow]$  is universal and it is same as that for the homogeneous electron gas. The exchange correlation energy functional of homogeneous electron gas is known, its exchange energy is calculated using simple analytic function and the correlation part is calculated using Monte Carlo simulations. Thus, the LSDA exchange correlation energy functional can be calculated. LSDA is a good approximation when the system is really homogeneous however, it is insufficient when the density of the system changes abruptly for example at the surface of the crystal.

### 2.6.2 The Generalized gradient approximation

The generalized gradient approximation(GGA) contains the density and the gradient of density at that point.

$$\begin{aligned} E_{xc}^{GGA}[n^\uparrow, n^\downarrow] &= \int d^3r n \vec{r} \epsilon_{xc}(n^\uparrow, n^\downarrow, |\nabla n^\uparrow|, |\nabla n^\downarrow|, \dots) \\ &= \int d^3r n(\vec{r}) \epsilon_x^{hom} F_{xc}(n^\uparrow, n^\downarrow, |\nabla n^\uparrow|, |\nabla n^\downarrow|, \dots) \end{aligned} \quad (2.127)$$

where  $\epsilon_x^{hom}$  exchange energy of the unpolarized gas and the  $F_{xc}$  is the dimensionless functional. For nonuniform charge densities GGA is more appropriate because it includes the gradient of density as well as the density itself at that point.

## 2.7 PSEUDOPOTENTIAL

In order to reduce the complexity of many body problem, the effect of core electrons can be replaced by a potential which is called pseudopotential. The core electrons in the atom are less affected from the change in the environment such as formation of a chemical bond. In addition, the valence state wavefunctions are rapidly oscillating near the core regions. It is obvious that the expansion of rapidly oscillating wavefunction in terms of planewaves is difficult. In order to make the wavefunction simple rapidly oscillating parts of the wavefunction should be replaced by a smoother wavefunction, which can be done by introducing a pseudopotential. Considering these discussions any valence state  $\psi$  can be written in terms of superposition of a smoother wavefunction  $\phi$  and the core states  $\chi_n$  [20].

$$|\psi\rangle = |\phi\rangle + \sum_n^{core} a_n |\chi_n\rangle \quad (2.128)$$

To find the  $a_n$ , above equation should be multiplied with  $\langle \chi_m |$ .

$$\langle \chi_m | \psi \rangle = \langle \chi_m | \phi \rangle + \sum_n^{core} a_n \langle \chi_m | \chi_n \rangle \quad (2.129)$$

The core states  $\chi_m$  are orthogonal to each other which means  $\langle \chi_m | \chi_n \rangle = \delta_{mn}$ , also the valence states are orthogonal to core states,

$$\begin{aligned} \langle \chi_m | \psi \rangle &= \langle \chi_m | \phi \rangle + \sum_n^{core} a_n \delta_{mn} \\ 0 &= \langle \chi_m | \phi \rangle + a_m \\ a_m &= -\langle \chi_m | \phi \rangle \end{aligned} \quad (2.130)$$

thus, the valance state can be written as

$$|\psi\rangle = |\phi\rangle - \sum_n \langle \chi_n | \phi \rangle |\chi_n\rangle \quad (2.131)$$

this equation is put into the single particle Schrödinger equation.

$$\begin{aligned} \hat{H}[|\phi\rangle - \sum_n \langle \chi_n | \phi \rangle |\chi_n\rangle] &= E[|\phi\rangle - \sum_n \langle \chi_n | \phi \rangle |\chi_n\rangle] \\ \hat{H}|\phi\rangle - \sum_n \langle \chi_n | \phi \rangle E_n |\chi_n\rangle &= E|\phi\rangle - E \sum_n \langle \chi_n | \phi \rangle |\chi_n\rangle \end{aligned} \quad (2.132)$$

When the similar terms are collectrd on the same side

$$\hat{H}|\phi\rangle - \sum_n (E_n - E) \langle \chi_n | \phi \rangle |\chi_n\rangle = E|\phi\rangle \quad (2.133)$$

Equation 2.133 can be written as

$$\left[-\frac{1}{2}\nabla^2 + \hat{V}_{ps}(\vec{r})\right]\phi(\vec{r}) = E\phi(\vec{r}) \quad (2.134)$$

This equation is the same as the single particle Schrödinger equation with smooth wavefunction. The pseudowavefunction gives the same eigenenergy with the real valance wavefunction. There are two different pseudopotentials in literature which are norm-conserving pseudopotential [21] and ultrasoft pseudopotential [22].

### 2.7.1 Norm-conserving pseudopotential

While generating norm conserving pseudopotential there are some properties that the pseudopotential and the pseudowavefunction should obey.

1. Real and the pseudo valance state wavefunction should agree in terms of eigenvalues for an atomic configuration.

$$\begin{aligned} [-\frac{1}{2}\nabla^2 + \hat{V}(\vec{r})]\psi(\vec{r}) &= E\psi(\vec{r}) \\ [-\frac{1}{2}\nabla^2 + \hat{V}_{ps}(\vec{r})]\phi(\vec{r}) &= E\phi(\vec{r}) \end{aligned} \quad (2.135)$$

2. Beyond a chosen core radius  $r_c$  the pseudo and the real wavefunction should be equal to each other.

$$\phi(\vec{r}) = \psi(\vec{r}) \quad \text{where } r \geq r_c \quad (2.136)$$

3. For  $r > r_c$  the integral of real and pseudo charge densities should be equal. This is the norm-conservation property.

$$\int_0^r |\phi|^2 r^2 dr = \int_0^r |\psi|^2 r^2 dr \quad (2.137)$$

4. The logarithmic derivative and the first energy derivative of the real wavefunction and the pseudowavefunction should be equal when  $r > r_c$

$$[(r\phi(\vec{r}))^2 \frac{d}{dE} \frac{d}{dr} \ln\phi(\vec{r})]_r = [(r\psi(\vec{r}))^2 \frac{d}{dE} \frac{d}{dr} \ln\psi(\vec{r})]_r \quad (2.138)$$

The last property improves the transferability of the pseudopotential. The norm-conservative pseudopotential is generated by solving the all-electron system considering above properties.

$$V_{ps}(\vec{r}) = \epsilon - \left[ \frac{l(l+1)}{2r^2} - \frac{\frac{d^2}{dr^2}\phi(\vec{r})}{\phi(\vec{r})} \right] \quad (2.139)$$

The  $r_c$  values are important while generating the norm-conservative pseudopotential. If  $r_c$  is small, the generated pseudopotential has good transferability. On the contrary, if  $r_c$  is large then the pseudopotential becomes smoother. To generate a good pseudopotential the  $r_c$  value should be chosen carefully.

### 2.7.2 Ultrasoft pseudopotentials

The difference between ultrasoft pseudopotential and the norm-conservative pseudopotential is the number of planewaves they use. While generating ultrasoft pseudopotentials the norm-conservation constraint is relaxed so it requires less planewaves than the norm-conserved pseudopotentials, that is why they are called ultrasoft.

## CHAPTER 3

### ELECTRONIC STRUCTURE ANALYSIS OF TiO<sub>2</sub> (001) ANATASE SURFACE

The metal oxides constitute a new and developing area of surface physics due to their wide range of applications in device physics and technology. Among these metal oxides TiO<sub>2</sub> become one of the most investigated materials in surface science. There are some properties that make TiO<sub>2</sub> such a desirable molecule, such as its ease of analysis by all kinds of experimental techniques, its wide range of applications, its low cost and biocompatibility [1].

#### 3.1 APPLICATION OF TiO<sub>2</sub>

The popularity of TiO<sub>2</sub> comes mainly from its wide range of applications. It is used as a photocatalyst in heterogeneous catalysis, gas sensor, white pigments, biomaterials, memory devices and optical coating. It is also used in solar cells, ceramics, electric devices and the new generation of metal oxide semiconductor field effect transistor (MOSFET) [1, 2].

##### 3.1.1 Photocatalysis application

TiO<sub>2</sub> is a very stable molecule under visible light, in this region it has no absorption so its color is white. However, TiO<sub>2</sub> becomes active when it is exposed to ultraviolet light because its band gap energy can be overcome by a photon in the ultraviolet region [23]. This activity can induce some chemical reactions on it which is called photocatalysis. The photocatalytic activity of matter is related to its ability of electron-hole pair production. The incoming photon excites an electron from valence band to the conduction band of TiO<sub>2</sub> which leads to a hole in the valence band and an electron in the conduction band. This electron-hole pair can start

the redox reaction with the molecules that adsorb on the surface of TiO<sub>2</sub> [24].

The first photocatalysis observation was done by mixing various organic solvents such as alcohol and hydrocarbons with TiO<sub>2</sub> powders under Hg lamp. After putting them together the autooxidation of solvents and the formation of H<sub>2</sub>O<sub>2</sub> was observed [25]. In addition, using this photocatalyst property of TiO<sub>2</sub> the water can be decomposed into oxygen and hydrogen without using any external voltage [26]. This hydrogen production from water and organic compounds, which are used for avoiding back reaction, is considered as a new energy source. However, TiO<sub>2</sub> can absorb only 3% of all spectrum due to its wide band gap. Thus, TiO<sub>2</sub> photocatalysis is not efficient for hydrogen production [23]. Due to this fact the direction of research was changed to the destruction of pollutants from water or air which can be done using TiO<sub>2</sub> powders [27]. It was reported that the stearic acid (C<sub>17</sub>H<sub>35</sub>O<sub>2</sub>) decomposed into CO<sub>2</sub> when it is coated on TiO<sub>2</sub> layer [28]. This observation suggests that the materials which are coated with TiO<sub>2</sub> can be kept clean. In addition, it has been shown that under standard conditions CO<sub>2</sub> could be transferred to methane gas when it interacts with TiO<sub>2</sub> pellets and with H<sub>2</sub>O under ultraviolet radiation so photocatalytic activity of TiO<sub>2</sub> can be used to reduce the CO<sub>2</sub> from the environment [29]. Another photocatalytic application of TiO<sub>2</sub> is its antibacterial effect. Especially when it is deposited with copper or silver an efficient and safe antibacterial effect is obtained even under weak ultraviolet light [30, 23, 31].

### 3.1.2 Solar cell applications

Another important application of TiO<sub>2</sub> is its usage as a component in solar cell technology. The first TiO<sub>2</sub> solar cell was made by a few nanometer thick film of optically transparent TiO<sub>2</sub> which is coated with light harvesting dye to transfer the charge. This dye-sensitized solar cell (DSSC) is also known as Grätzel cell [5].

The widely used semiconductor solar cells are made of silicon based p-n junctions. The p-n silicon junction is obtained by combining the p-type and n-type silicons together. The DSSC are good alternatives to p-n junction photovoltaic devices economically. In p-n junction solar cells the light absorption and the charge transfer occurs at the same place, however, in DSSC these two operations happen at different places; the light is absorbed by a dye molecule and charge transfer is done to the wide band gap semiconductor. The light excites the electron of the dye to its conduction band. Then, the excited electron is directly diffused to the conduction

band of the TiO<sub>2</sub> which has lower energy than lowest unoccupied molecular orbital (LUMO) of the light harvesting dye molecule. The missing electron of the dye is supplied by the electrolyte solution immediately. The conducting glass and the cathode plate is linked with a wire so that the electron in the TiO<sub>2</sub> conduction band can complete the circuit. In conclusion, without any permanent chemical transformation, the electrical energy can be produced [32, 33].

In order to get an efficient photovoltaic or photocatalytic device, the absorbed light portion of solar spectrum by the dye-TiO<sub>2</sub> systems should be increased by decreasing the band gap energy of these systems [34, 35]. This can be done by doping transition metal ions (Cr, Fe, Ni) inside TiO<sub>2</sub> [36], creating oxygen vacancies, or coating TiO<sub>2</sub> with the light harvesting dye molecules [37, 38].

## **3.2 DENSITY FUNCTIONAL THEORY CALCULATIONS OF ANATASE (001) SURFACE**

### **3.2.1 Crystal structure of TiO<sub>2</sub>**

In nature TiO<sub>2</sub> occurs in mainly three different crystal structures: rutile, anatase, and brookite [39]. There are also some high pressure forms such as monoclinic baddeleyite [40] and orthorhombic  $\alpha$  - PbO<sub>2</sub> [41].

#### **3.2.1.1 Rutile**

Rutile is the most common and stable form of TiO<sub>2</sub>, meaning the other crystal forms can be converted to rutile by heating [42]. The rutile has tetragonal unit cell as shown Fig. 3.1, where the grey balls are titanium atoms and the red ones are oxygens. The cell parameters of rutile form of TiO<sub>2</sub> are  $a = b = 4.584 \text{ \AA}$  and  $c = 2.953 \text{ \AA}$  [1]. According to ab initio calculations, (110) surface of rutile has the lowest surface energy and the (001) has the highest surface energy. The other surfaces have energies between these values [43]. Thus (110) surface of rutile is the most stable surface.

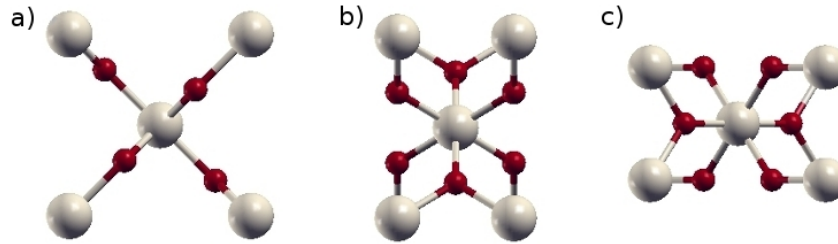


Figure 3.1: Unit cell of  $\text{TiO}_2$  in rutile form, (a) front view, (b) side view, and (c) top view

### 3.2.1.2 Anatase

Anatase is another crystal form of  $\text{TiO}_2$ . Similar to rutile, it has tetragonal unit cell (Fig. 3.2) and its cell parameters are  $a = b = 3.782 \text{ \AA}$  and  $c = 9.502 \text{ \AA}$  [1]. The anatase form of  $\text{TiO}_2$  are used especially in photocatalytic and photovoltaic applications. The photocatalytic reactions become more efficient when the powder is a mixture of anatase and rutile forms with a ratio of 3:1 [44].  $\text{TiO}_2$  nanoparticels whose sizes up to  $14 \text{ \AA}$  do not occur in the rutile form, but instead they form a metastable anatase form [2]. Thus, most of the photovoltaic cells contain anatase form of  $\text{TiO}_2$ .

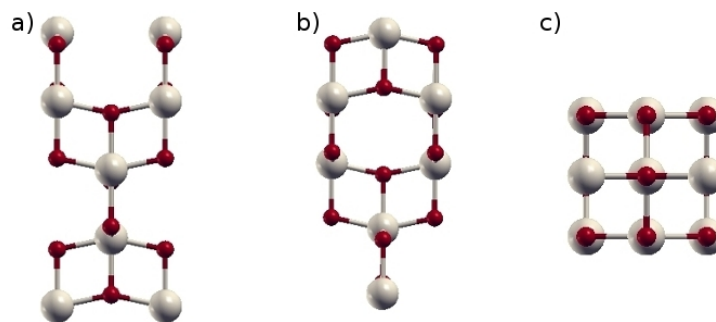


Figure 3.2: Unit cell of  $\text{TiO}_2$  in anatase form, (a) front view, (b) side view, and (c) top view

### 3.2.1.3 Brookite

The third well known  $\text{TiO}_2$  structure is brookite. Unlike the other forms, brookite has rhombohedral unit cell with cell parameters  $a = 5.436 \text{ \AA}$ ,  $b = 9.166 \text{ \AA}$  and  $c = 5.135 \text{ \AA}$ .

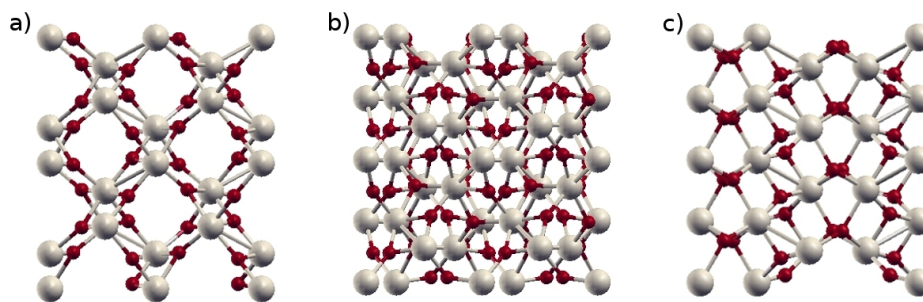


Figure 3.3: Unit cell of  $\text{TiO}_2$  in brookite form, (a) front view, (b) side view, and (c) top view

Compared to other forms brookite form of  $\text{TiO}_2$  can be found rarely; and also it does not have photocatalytic activity. [1].

### 3.2.2 Bulk calculations

The efficiency of DSSC depends on both the dye molecules and the semiconductor materials used. The most commonly used semiconductor is  $\text{TiO}_2$ , but other wide band gap semiconductors that are also used such as  $\text{ZnO}$  and  $\text{Nb}_2\text{O}_5$  [45]. In addition to the semiconductor kind, the crystal structure of semiconductor is also important. The anatase form of  $\text{TiO}_2$  is more favorable than other modifications of  $\text{TiO}_2$  in solar cell applications because the anatase have largest surface area among crystal structures of  $\text{TiO}_2$ . According to the absorption spectra of  $\text{TiO}_2$  films, the dye molecules can adsorb on anatase 35 % more than other crystal forms [46]. Thus, in this work the adsorption of aromatic rings, which are the component of dye molecule, on the  $\text{TiO}_2$  anatase surface is considered for solar cell applications.

In order to analyse the electronic properties of anatase  $\text{TiO}_2$  the lattice parameters of the tetragonal unit cell of anatase bulk should be calculated. As it was stated before the real lattice parameters of anatase bulk are  $a = b = 3.782 \text{ \AA}$  and  $c = 9.502 \text{ \AA}$ . The lattice parameters were calculated using an extended Lagrangian algorithm which is based on cell relaxation [47]. In order to find the optimum positions of the atoms, the algorithm changes the coordinates of each atom and size of the unit cell until the total force on each atom is less than a tolerance value which is taken as  $10^{-4} \text{ Ry/au}$  in this work. Another important convergence parameter

is set for the total energy. The relaxation procedure consists of numerous self consistent field (SCF) calculations. Every SCF calculation ends with a converged total energy value of the system. If the energy difference between two consecutive SCF steps is less than the total energy convergence threshold then the convergence criteria is satisfied. In this work total convergence threshold is taken to be  $10^{-4}$  Ry. In order to obtain optimum atomic coordinates successfully both criteria must be satisfied.

While doing the bulk calculations  $6 \times 6 \times 6$  k-point mesh is used. This k-point set causes 32 k-points in reciprocal space, so total energy is calculated at these 32 k-points. After satisfying both of the convergence criteria, the lattice parameters are found  $a = b = 3.808 \text{ \AA}$  and  $c = 9.5146 \text{ \AA}$ , and the volume of unit cell is  $136.25 \text{ \AA}^3$ . The calculated lattice parameters agree with experimental values upto 0.6% for  $a$  and  $b$ , 0.12% for  $c$ .

The density functional theory calculations are made using PWSCF (Plane-Wave Self-Consistent Field) code of Quantum - ESPRESSO package [48]. Moreover, the GGA-PBE exchange-correlational functional and the ultrasoft pseudopotentials are used [49, 22]. Well-converged results were obtained for 35 Ry kinetic energy cut off and 350 Ry augmentation charge density cutoff.

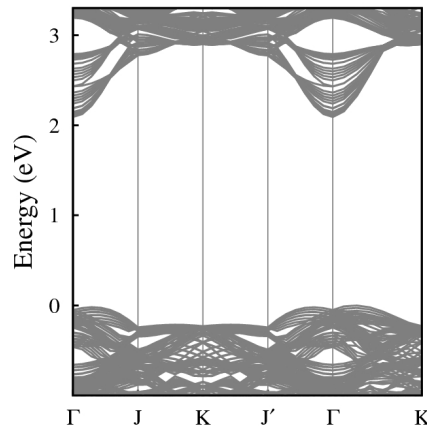


Figure 3.4: Projected band structure of anatase bulk

Fig. 3.4 shows the electronic energy band structure of TiO<sub>2</sub> anatase bulk crystal projected on the surface Brillouin zone (SBZ) for the (001) 2 × 2 surface reconstruction. Energy band structure supplies very important information about the electronic properties of the system. The energy levels of electrons which are bound to an atom are discrete, however, when lots of atoms come together the degenerate atomic orbital levels are split and they form molecular orbitals. The energy interval between these molecular orbitals is so small that they are considered as a continuum, namely, bands. Then, if the energy of electron is calculated at consecutive k-points, the dispersed band structure is obtained. The projected band structure is determined as the projection of the 3D reciprocal lattice to 2D reciprocal lattice by calculating energy values for the same direction with different  $k_z$  points, then project them on the same plot. In this work, the direction of reciprocal space is defined as

$$\Gamma(000) \rightarrow J(010) \rightarrow K(110) \rightarrow J'(100) \rightarrow \Gamma(000) \rightarrow K(110). \quad (3.1)$$

The energy region where there is no state is called the band gap. The energy band gap is defined as the energy difference between the valance band top and the conduction band bottom of the crystal so it is also equal to the energy that is needed to make the outer shell electrons free. The experimental band gap value of TiO<sub>2</sub> anatase is 3.2 eV, however, the band gap value obtained using DFT in this work for this system is only about 2.1 eV. This underestimation of the gap is due to an artifact of the DFT method.

### 3.2.3 Surface calculations

In the real world every crystal structure should have a surface because actually there is no ideal bulk which can grow to infinity in nature. Thus, analyzing the surface properties of crystals will be more reasonable. Especially nanomaterials have different and great properties than their bulk phases such as TiO<sub>2</sub> nanoparticles which is used in photocatalysis, photovoltaic, photonic crystals and sensing. In addition, different facets of the surface have different properties. The most stable facet of TiO<sub>2</sub> anatase is (101) surface, however, the chemically more active facet is (001) surface [8]. The (001) crystal facets have great importance in the reactivity of anatase nanoparticles [2]. Additionally, according to the recent studies TiO<sub>2</sub> anatase nanosheets exhibit 89% (001) facets and high photocatalytic properties [9]. Due to these reasons throughout this work TiO<sub>2</sub> anatase (001) surface is investigated.

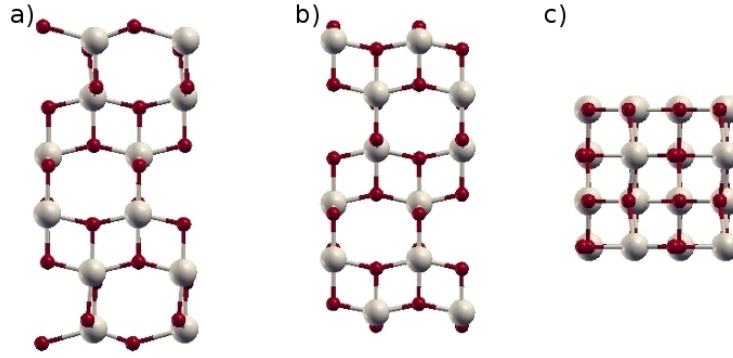


Figure 3.5: The anatase slab which is used in this work a) Front view, b) Side view, c) Top view

The surface studies are done in a 6-layer slab (Fig. 3.5) and the initial stoichiometric slab which has 72 atoms is directly obtained from bulk  $\text{TiO}_2$  by truncation. The optimum atomic positions of the slab and the bulk  $\text{TiO}_2$  are different due to the surface reconstruction. Surface structure leads to extra forces on atoms that are especially close to the surface due to their unsaturated bonds. In order to get rid of these extra forces a relaxation procedure is performed. During relaxation procedure the atoms in the slab are not fixed, but free to move until the forces on each atom is diminished down to  $10^{-4}$  Ry/au. The distance between oxygen atoms and the nearest neighbor titanium atoms is equal  $1.93 \text{ \AA}$  in the bulk. However, after the relaxation procedure the oxygen atoms on the top of the slab slide through one of the nearest neighbor titanium atom. Thus, distances between oxygen atoms and the nearest neighbor titanium atoms are unequal, one of them shortens to  $1.74 \text{ \AA}$  and the other elongates to  $2.23 \text{ \AA}$  as shown in Fig. 3.6. For the surface relaxation procedure  $3 \times 3 \times 1$  k-point mesh is used. The total energy of the slab is calculated for these five special k-points. In order to determine the positioning of the surface states clearly the surface band structure is plotted on the projected bulk band structure (Fig. 3.7). The states which are in the band gap of the bulk anatase above the valance band are coming from the dangling bonds of the surface. Due to this surface states the band gap of the system is decreased to approximately  $1.9 \text{ eV}$ . The states may be chosen at an arbitrary k-point, say  $\Gamma$ , and their partial charge density,  $|\psi|^2$  can be depicted for each band. Fig. 3.8 shows the twofold degenerate states (coming from both surfaces of the slab) above the valance band falling into the gap are localized on the surfaces.

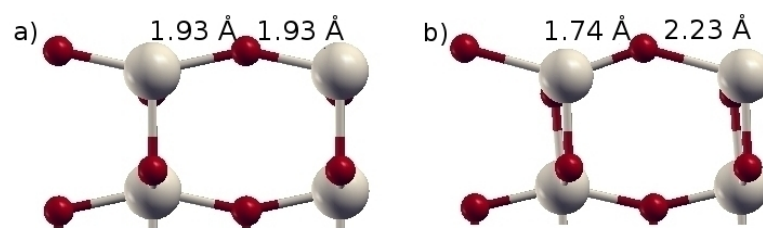


Figure 3.6: Distance between oxygen atom and the titanium atoms at the surface of slab (a) before and (b) after relaxation

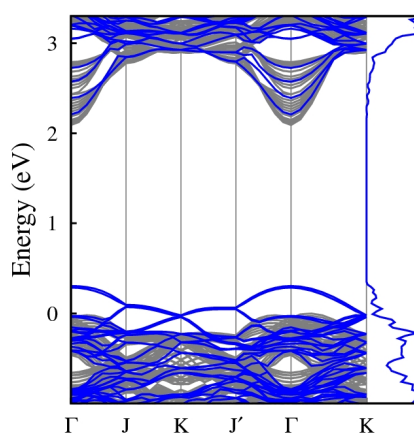


Figure 3.7: Anatase (001) surface bands projected on bulk band structure

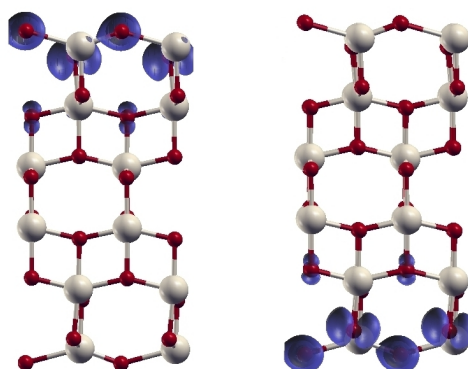


Figure 3.8: Partial charge densities of surface states at  $\Gamma$

## CHAPTER 4

# ELECTRONIC STRUCTURE ANALYSIS OF AROMATIC MOLECULES, ADSORBED ON TiO<sub>2</sub> (001) ANATASE SURFACE

In order to obtain an efficient photovoltaic device, the absorbed light portion of solar spectrum by TiO<sub>2</sub> based systems should be increased. This can be supplied by attaching covalently the functional aromatic molecules which are called dye molecules, on the TiO<sub>2</sub> surfaces [50]. Aromatic rings, which are the backbones of many dye molecules are a convenient means of modelling the main ingredients of their working principle. However, due to their inertness, the chemical adsorption of these aromatic rings to the underlying substrate can only be achieved through an anchor molecule such as formic acid, phosphonic acid or  $\beta$ -diketones groups [4]. Anchor group molecules also supply electron transfer from the dye molecules to the TiO<sub>2</sub> surface [10].

### 4.1 ADSORPTION OF ANCHOR GROUP MOLECULES

The anchor group molecules play an important role in designing solar cells and optoelectronic devices which need ultrafast surface electron transfer. The most widely used anchor groups are formic (carboxylic) acid and phosphonic acid.

#### 4.1.1 Formic acid adsorption

Formic acid is the most widely used and the simplest carboxylic acid with the chemical formula of R-COOH, where R can be replaced by a hydrogen atom or any aromatic molecule.

The most efficient dye sensitized solar cells are designed by using ruthenium dyes which contain formic acid anchor groups supplying good electron transfer from aromatic adsorbate to the wide-gap semiconductor [51].

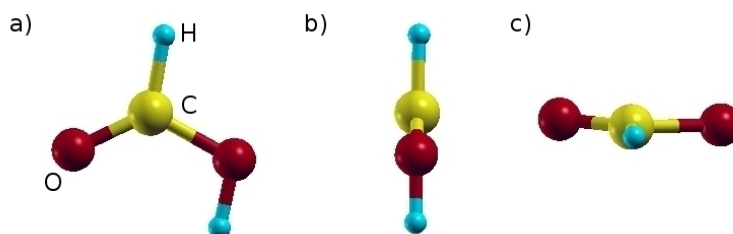


Figure 4.1: Formic acid molecule (a) front view, (b) side view and c) top view.

The relaxed structure of formic acid can be seen in Fig. 4.1. Here the dark red balls represent oxygen atoms, the blue small ones are hydrogens and the light yellow one is the carbon. The hydrogen connected to carbon can be replaced by aromatic adsorbates.

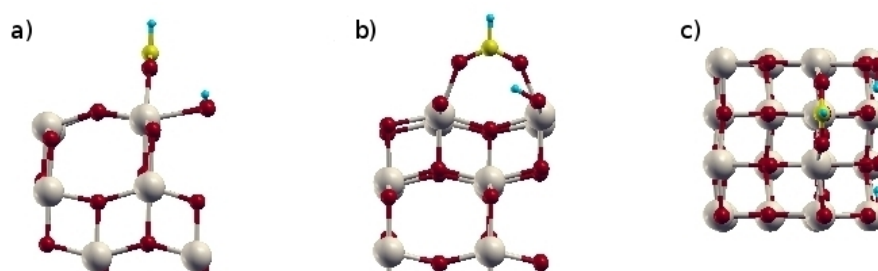


Figure 4.2: Formic acid adsorption on  $\text{TiO}_2$  anatase (001)  $2 \times 2$  surface (a) front view (b) side view and (c) top view.

The formic acid molecules are adsorbed symmetrically on both of the surfaces of the six layer symmetrical  $\text{TiO}_2$  slab (only half of which) is shown in Fig. 4.2. The symmetric adsorption configuration is preferred in order to prevent unequivalent band gap states from the each sur-

face but obtain identical (degenerate) surface bands from both. After geometric optimization the two oxygens of the formic acid bonds to the two titanium atoms of the reconstructed surface. In addition, the hydrogen of OH group in formic acid breaks away from the molecule and bonds to a surface oxygen. The main contribution of the formic acid to the band structure of the system (Fig. 4.3) is to the states which are in the vicinity of valence band top, the oxygen-titanium interaction does not bring any localized states into the energy band gap. Thus, formic acid can not functionalize the anatase surface by itself because it can not narrow the band gap, but is rather used binding other functional groups to the semiconductor surface.

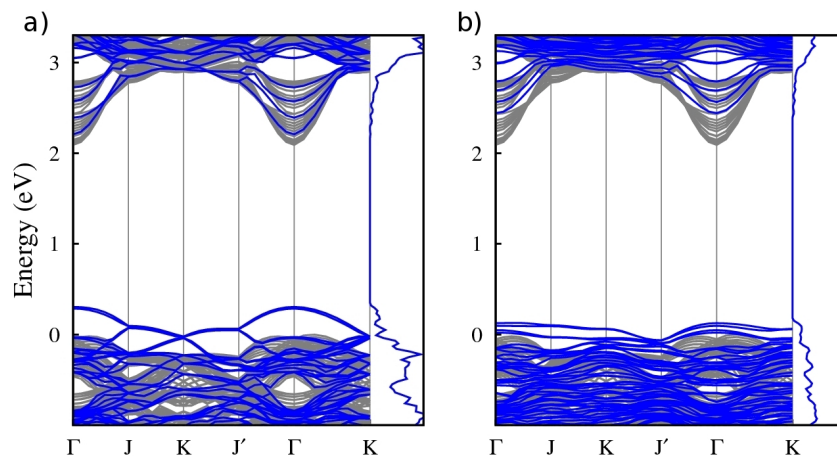


Figure 4.3: Band structure along the symmetry lines of the surface Brillouin zone and density of states of (a) clean  $\text{TiO}_2$  surface (b) formic acid adsorbed on anatase (001) surface. Shaded region shows the bulk band projected on the same surface Brillouin zone. The top of the bulk valence band is taken to be zero.

Due to the saturation of dangling bonds on the surface by adsorbing the formic acid, the surface states disperse through the valence band continuum. Thus, the band gap of the system increased comparing with the clean surface. The band gap value of this configuration is found as 2.31 eV. The contribution of formic acid to the total density of states can be seen in Fig. 4.4 by calculating the molecule's partial density of states. Another important information is that the binding energy of molecules. Binding energy gives an idea about how strong the molecule

is adsorbed on the surface. It is formulated as:

$$E_{\text{binding}} = E_{\text{molecule+slab}} - (E_{\text{slab}} + E_{\text{molecule}}) \quad (4.1)$$

where  $E_{\text{molecule}}$ ,  $E_{\text{slab}}$ , and  $E_{\text{molecule+slab}}$  are the total energies of the isolated molecule, clean slab, and the combined system which are all relaxed. According to 4.1 the binding energy of formic acid is found as  $-3.05$  eV.

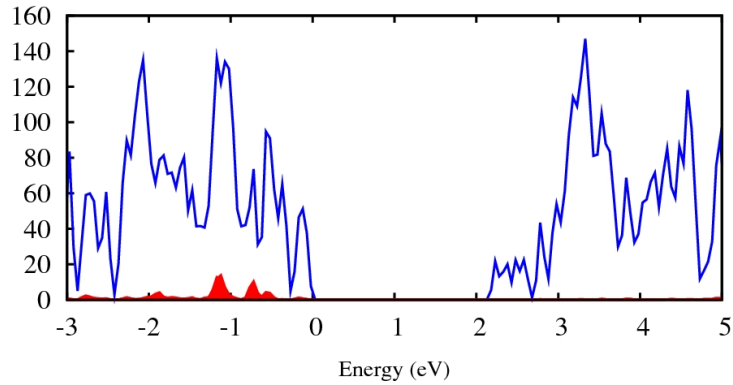


Figure 4.4: Density of states of the whole system (blue line) and the partial density of states due to the formic acid (shaded in red)

#### 4.1.2 Phosphonic acid adsorption

Phosphonic acid is another promising alternative anchor group, which binds to the  $\text{TiO}_2$  surface more strongly than the formic acid, with the chemical formula of  $\text{R-PO}_3\text{H}_2$  [50]. In addition, phosphonic acid supplies long term stability because it desorbs relatively slowly in the presence of water compared to formic acid [52]. The optimized structure of phosphonic acid can be seen in Fig. 4.5, the red dark balls are oxygens, the blue small ones are hydrogens and the green light big one is the phosphorous. The hydrogen bonded to phosphorous, just like in the formic acid case, can be replaced by aromatic adsorbates. The phosphonic acid is adsorbed on  $\text{TiO}_2$  anatase (001) surface which we modelled by a six-layer slab (Fig. 4.6). The two oxygen of the anchor group are attached to the titanium atoms of the reconstructed

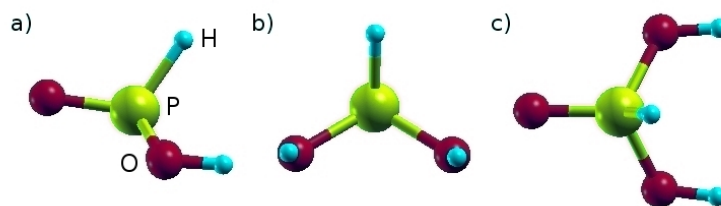


Figure 4.5: Phosphonic acid a) Front view b) Side view c) Top view

surface. These bond formations help saturating the dangling bonds on the surface remove the surface bands in the gap (Fig. 4.7a), acid push them into the valence band ((Fig. 4.7b)). In addition, the two namely flat bands appear in the gap ((Fig. 4.7b)), however, they have different origin namely due to the rest of the acid. The nature of these states can be identified using partial density of states which can give the contribution of atoms to the total density of states of the system.

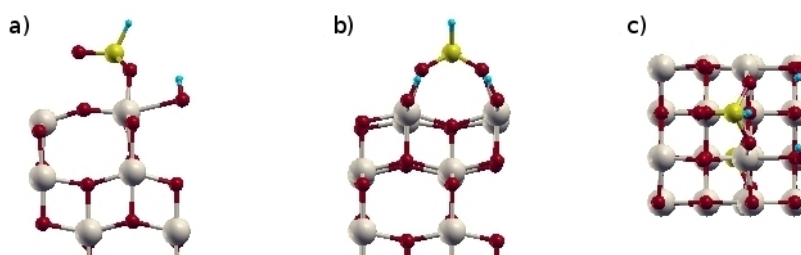


Figure 4.6: Phosphonic acid adsorption on  $\text{TiO}_2$  anatase (001) surface. (a) Front view, (b) side view, and c) top view

Partial density of states calculations shows that (Fig. 4.8) the  $p$ -orbitals of the oxygen atoms and the  $s$ -orbital of the hydrogen atom bonded to phosphorous are responsible for the extra states in the band gap. The band gap is decreased to 1.64 eV for this case. The nature of these states can also be verified by visualizing the partial charge density. Fig. 4.9 shows that the electron probability density for each of these gap states is localized around the adsorbed molecule and has no contribution from the substrate. The binding energy of phosphonic acid is calculated to be 4.384 eV, and it is bigger than the binding energy of the formic acid, so, phosphonic acid binds more strongly than formic acid on  $\text{TiO}_2$  anatase (001) surface.

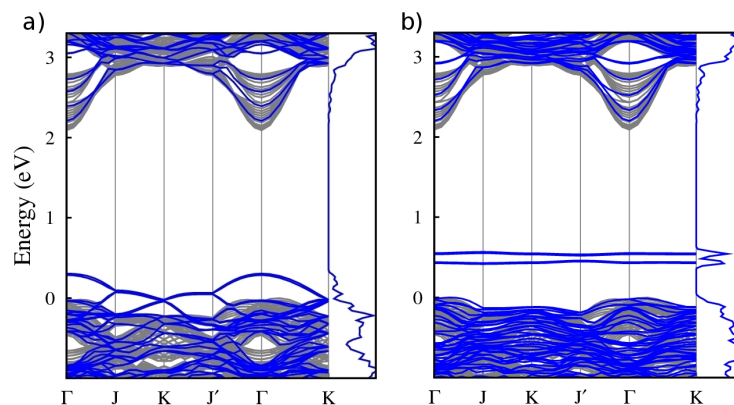


Figure 4.7: Band structure along the symmetry lines of the surface Brillouin zone and density of states of (a) Clean surface and (b) Phosphonic acid adsorbed on anatase (001) surface. Shaded region shows the bulk band projected on the same surface Brillouin zone. The top of the bulk valence band is taken to be zero.

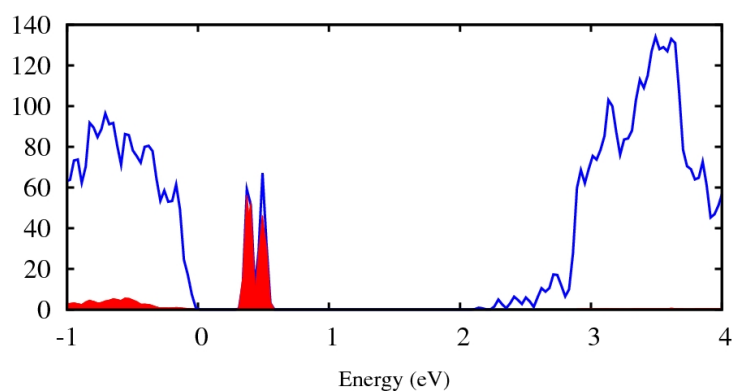


Figure 4.8: Density of states of the whole system (blue line) and the partial density of states due to the phosphonic acid (shaded in red).

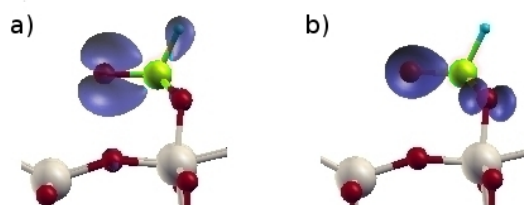


Figure 4.9: Charge density plots for (a) the upper lying gap state and (b) the lower lying gap state.

## 4.2 AROMATIC RING ADSORPTION ON ANATASE (001) SURFACE

In photocatalysis and photovoltaic researches identified so far  $\text{TiO}_2$  appears to be the most appropriate material among other semiconductors. Due to its wide band gap,  $\text{TiO}_2$  can absorb wavelengths below 400 nm, which corresponds to ultraviolet region of the spectrum. However, the wavelength range of the sun coming to the earth is 300–2000 nm. Thus, in order to get an efficient photovoltaic device, the adsorbed light portion of the  $\text{TiO}_2$  system should be increased. This problem can be handled by coating the  $\text{TiO}_2$  surface with dye material such as aromatic and polyaromatic compounds, transition metal polypyridine complexes and carotenoid compounds [3, 4]. It is observed that  $\text{TiO}_2$  film electrodes coated with a monolayer of dye (photosensitizer) molecules can produce higher photocurrents than electrodes without dye molecules [5].

The early works showed that the organic dyes on  $\text{TiO}_2$  give a relatively low solar energy to electricity conversion efficiency which is of about 1.3 % only. However, recent studies on organic dyes have improved this by far. The merocyanine organic dye which contains carboxylic acid as anchor to the surface of the semiconductor was observed to show a high efficiency of about 4.2 % [6]. Organic coumarin dye derivatives can absorb light in the 400–700 nm wavelength region, with an efficiency of up to 5.6 % [7]. This progress encouraged the researchers to look for more efficient organic dyes.

In this work, the electronic structure of the simplest linear series of aromatic rings adsorbed on  $\text{TiO}_2$  (001) anatase surface is investigated. These aromatic rings which are the components of organic dye molecules, are anchored on  $\text{TiO}_2$  (001) anatase surface via carboxylic acid and phosphonic acid. The goal is to find a trend as a function of number of rings which is expected to be an important step in designing a setup with a controllable parameter.

### 4.2.1 Adsorption of aromatic rings anchored by formic acid

The linear series of aromatic rings are anchored on anatase (001) surface using formic acid as shown in Fig. 4.10. The geometric structure of the surface is found to be not affected by the addition of aromatic rings. Moreover, the distance between aromatic rings and the surface are also not affected by the addition of aromatic rings. The distance between rings and the surface is found to be 2.08 Å. The aromatic rings are made to adsorb on both surfaces of the

slab symmetrically, in order to get degenerate molecular energy levels in the band structure of the system. The effect of the aromatic rings on the electronic structure of the system is analyzed by using aromatic molecules which have up to five aromatic rings. The band structures and the density of states of these systems are shown, in Fig. 4.10 are shown in Fig. 4.11(a) to (f), respectively. When the aromatic molecules which have one aromatic ring are adsorbed on the surface (Fig. 4.10(b)) with formic acid as the anchor, a flat going extra state appears in the band gap shown in (Fig. 4.11(b)). This state occurs approximately 0.1 eV above the valence band top of the previous system and due to this gap state the band gap of the system is decreased to 2.18 eV.

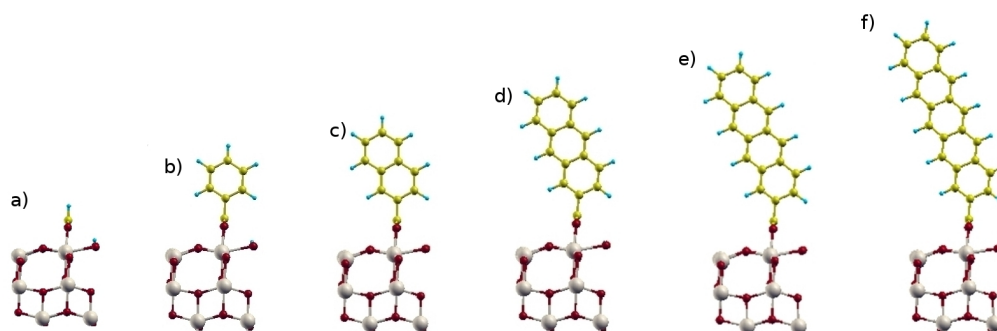


Figure 4.10: Geometry optimized  $\text{TiO}_2$  anatase (001)  $2 \times 2$  surfaces with varying number of aromatic rings anchored via formic acid

When the second ring is attached shown in Fig. 4.10(c), another extra gap state is introduced approximately 0.7 eV above the previous state as shown in Fig. 4.11(c). Due to this state the band gap of the system is decreased further to 1.46 eV. With the introduction of the third ring, this trend is broken. When the aromatic molecules which have three aromatic rings (naphthalene) are adsorbed on the surface in Fig. 4.10(d), no extra gap states occur in addition to the states in the two-ring system. In this case, the upper lying gap state seems to move upward towards the conduction band edge (CBE), approximately 0.5 eV, thus the band gap of the system is now decreased to 0.95 eV (Fig. 4.11(d)). In the four-ring case, shown in Fig. 4.10(e), there are three states in the band gap. In addition to the extra states in three-ring case, another state emerges below the states existing in the previous case, which are as a result pushed up to higher energies. This causes the band gap of the system to become 0.61 eV (Fig.

4.11(e)). In the five-ring case, (Fig. 4.10(f)) the band gap is further reduced and has become 0.35 eV, as can be seen in Fig. 4.11(f).

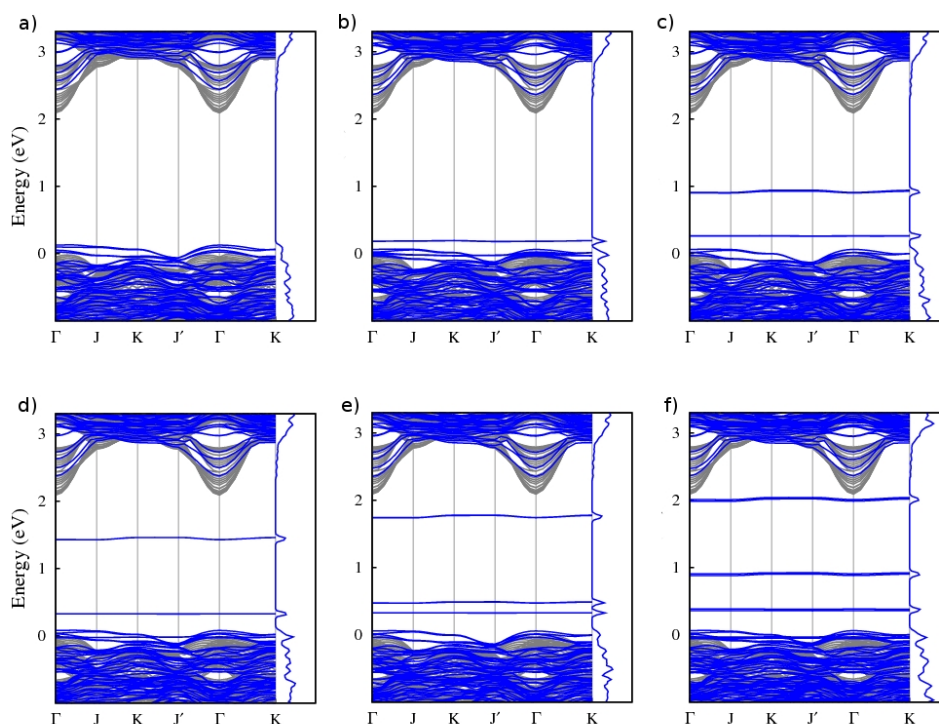


Figure 4.11: Band Structures of aromatic ring adsorption on anatase (001) surface anchored via formic acid. (a) Formic acid adsorbed system, and the number of rings in figures (b), (c), (d), (e), (f) are 1, 2, 3, 4, 5 respectively

In order to verify the origin of the gap states as molecular, a partial charge density analysis is conducted by plotting the norm square of the Kohn-Sham orbitals for a k-point along the highest occupied dispersionless band. As seen in Fig. 4.12 these states are found always to be localized around the molecule verifying that they are introduced into the gap by the molecule. The contribution of the molecules to the electronic structure of the system can be identified by using partial density of states calculation. The total density of states of each system is displayed as blue line and the contribution of the molecule to the density of state is displayed as shaded in red in Fig. 4.14 from one-ring to five-ring, respectively. The density of

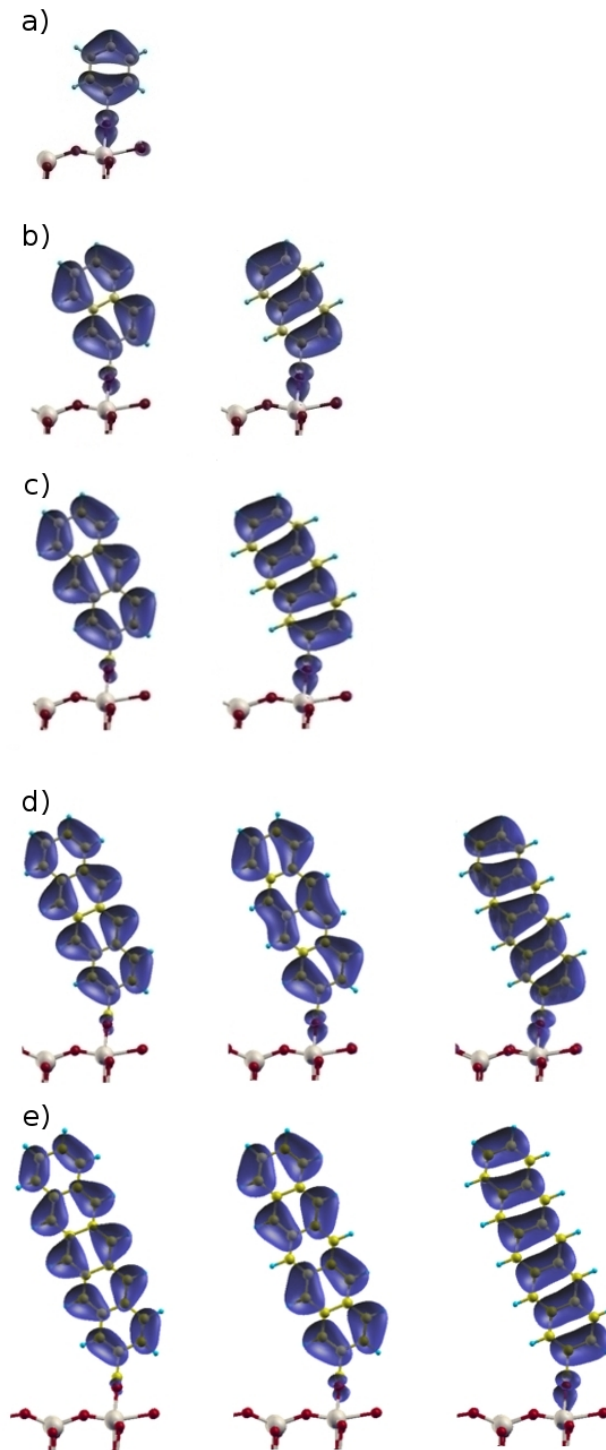


Figure 4.12: Partial charge densities for the gap states at  $\Gamma$  point. The number of rings in figure (a) , (b), (c), (d), (e) are 1, 2, 3, 4, 5 respectively. The first plot in (b) and (c) corresponds to the upper lying gap state, the second one corresponds to the lower lying gap state. In (d) and (e) the first plot corresponds to the upper lying gap state, the second one corresponds to the state which is in the middle and the third one corresponds to the lower lying gap state

states in negative energies belongs to the valence band and positive energy region includes the gap and the conduction band of the system. According to the partial density of states calculation the highest occupied molecular orbital (HOMO) of the system belongs to the *p*-orbitals of the carbon rings (Fig. 4.14).

The lowest unoccupied level of the molecule (LUMO) whose position is important for several photovoltaic applications, can also be identified by using partial density of state analysis, which is in the conduction band of the system. The energy gap between HOMO and the LUMO levels of the molecule is 4.76 eV, shown in Fig. 4.14(a) for the system which has one aromatic ring. In the two-ring case, in addition to the displaced HOMO level, the LUMO level of the molecule also moves up to the CBE, so the energy gap between them is decreased to 3.40 eV. This trend continues for the other systems, the energy gap between HOMO and LUMO levels become 2.35 eV for the three ring system, 1.65 eV for the four-ring system and about 1.15 eV for the five ring system. The decrease in HOMO–LUMO energy difference can be seen in Fig. 4.13. The binding energy of the molecules is also important for the stability of the system. These values and the other electronic properties of adsorbed molecules are listed in Table 4.1.

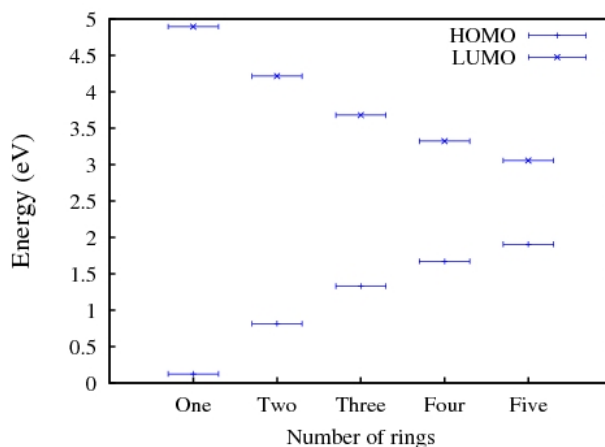


Figure 4.13: HOMO–LUMO energy differences of adsorbed molecules versus the number of aromatic rings

#### 4.2.2 Adsorption of aromatic rings anchored by phosphonic acid

The linear series of aromatic rings are anchored on surface using phosphonic acid as in Fig. 4.15. Similar to the previous analysis, the electronic structure of aromatic rings are analyzed

Table 4.1: Binding energy and the gaps for each system with formic acid as the anchor.

	Binding energy (eV)	HOMO–LUMO Gap (eV)	HOMO–CBE gap (eV)
Clean surface	-	1.90	1.90
Formic acid	-3.05	7.00	2.31
One-ring	-2.37	4.76	2.18
Two-ring	-2.59	3.40	1.46
Three-ring	-2.70	2.35	0.95
Four-ring	-2.88	1.65	0.61
Five-ring	-3.11	1.15	0.35

up to five aromatic rings. The distance between rings and the surface is found to be as 4.03 Å. The aromatic rings are adsorbed on both surface of the slab symmetrically like in formic acid case (Fig. 4.15). The band structure and the density of states of the systems are shown in Fig. 4.15 can be seen in Fig. 4.16(a) to (f) respectively.

When the molecules which have one aromatic ring are adsorbed on surface, four flat going extra state appears in the band gap, shown in Fig 4.16(b). Due to these states the band gap of the system is decreased to to 1.64 eV. When the aromatic molecules have two aromatic rings, the upper lying gap state seems to move upward towards higher energies. Thus, the band gap become to 0.90 eV. In the third-ring case, in addition to the states in the previous system, another extra gap state emerges in the band gap and the upper lying gap state shift through the CBE. Thus, the band gap energy is decreased to 0.56 eV.

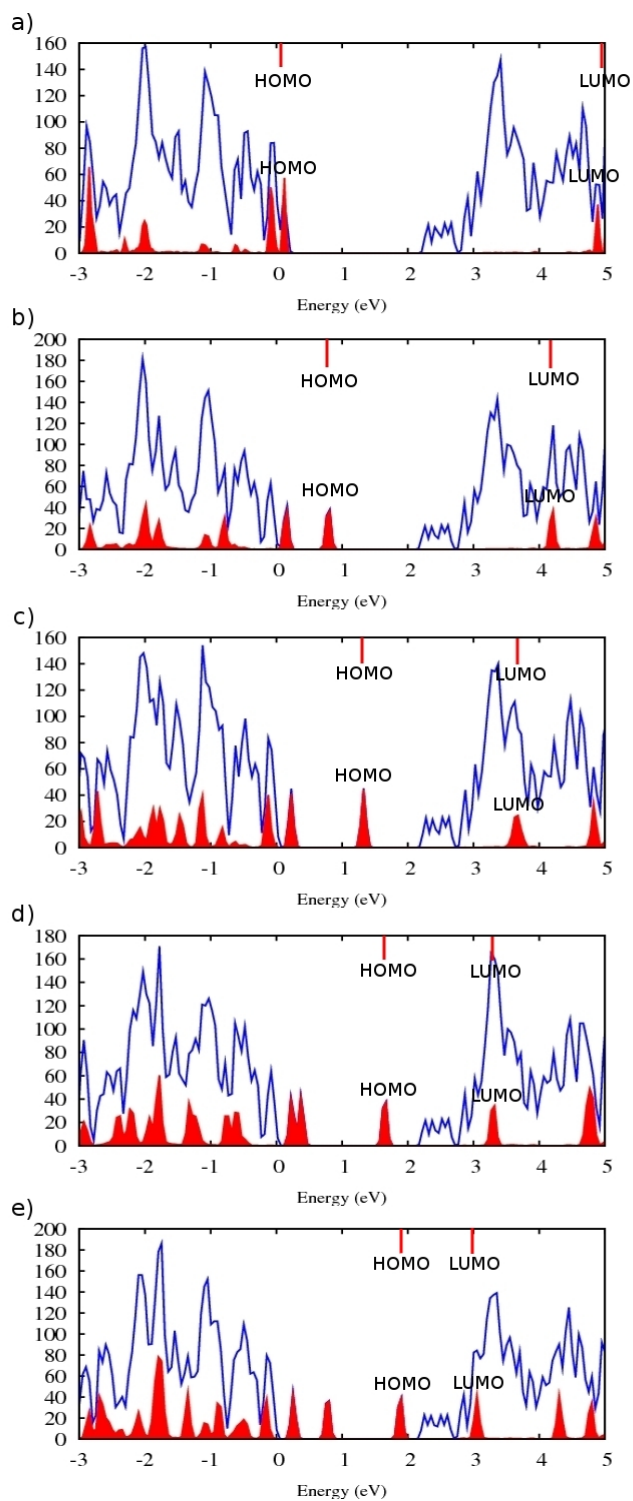


Figure 4.14: Contribution of molecule's partial density of states to the total density of states. Valence band top of the bulk projection is at 0 eV. The number of rings in figure (a), (b), (c), (d), (e) are 1, 2, 3, 4, 5 respectively. The HOMO and the LUMO level of the isolated rings is shown above the each of the panel.

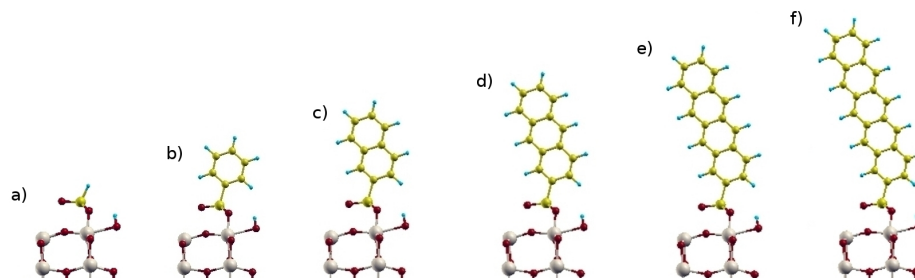


Figure 4.15: Geometry optimized  $\text{TiO}_2$  anatase (001)  $2 \times 2$  surfaces with varying number of aromatic rings anchored via phosphonic acid

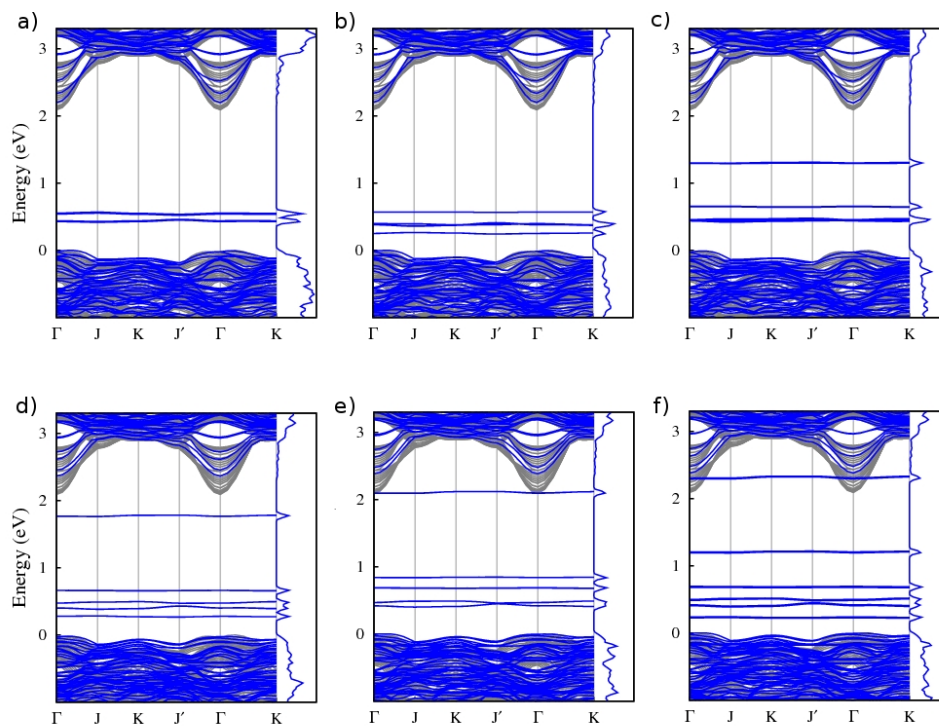


Figure 4.16: Band Structures of aromatic ring adsorption on anatase (001) surface anchored via phosphonic acid. (a) Phosphonic acid adsorbed system, and the number of rings in figures (b), (c), (d), (e), (f) are 1, 2, 3, 4, 5 respectively

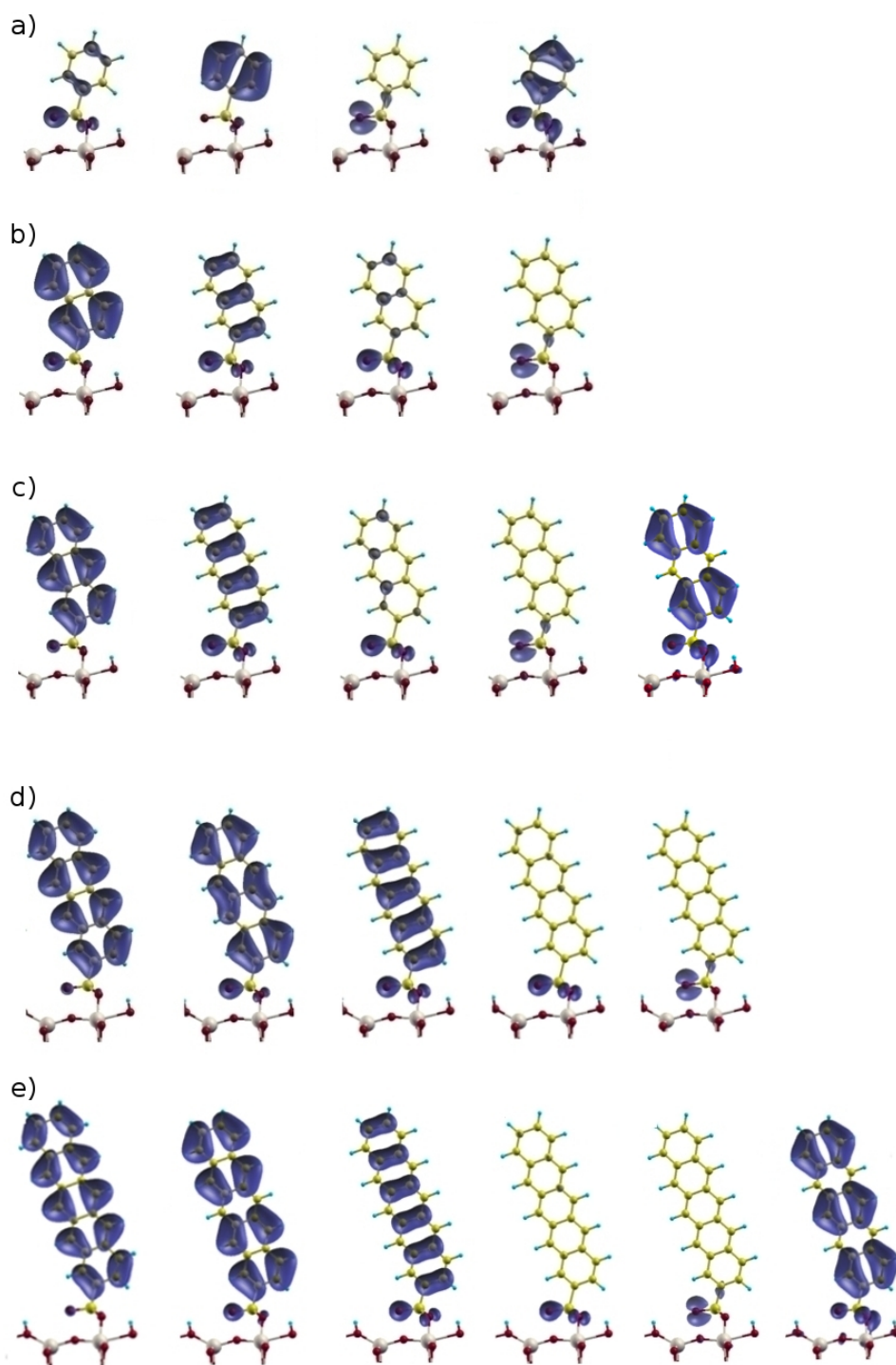


Figure 4.17: Partial charge densities for the gap states at  $\Gamma$  point. The number of rings in figure a,b,c,d,e are 1,2,3,4,5 respectively. The first plot in a, corresponds to upper lying gap state in Fig. 4.16(b), the second and the third one corresponds to middle gap state and the final one corresponds to lower lying gap state. The plots in figure b,c,d,e are the partial charge densities of gap states in Fig. 4.16(c),(d),(e) and ordered as above respectively

The contribution of molecules to the total density of states is shown in Fig. 4.18. Similar

Table 4.2: Binding energy and the gaps for each system with phosphonic acid as the anchor

	Binding energy (eV)	HOMO–LUMO Gap (eV)	HOMO–CBE gap (eV)
Clean surface	-	1.9	1.9
Phosphonic acid	-4.38	7.00	1.65
One-ring	-3.20	4.54	1.64
Two-ring	-4.00	3.35	0.90
Three-ring	-3.95	2.30	0.56
Four-ring	-5.12	1.62	0.29
Five-ring	-4.36	1.15	0.10

to the formic acid case the energy gap between HOMO and LUMO levels of the molecule decreases when the number of rings in the molecule is increased. In the one ring-case, the gap between HOMO and LUMO levels is 4.54 eV and it decreases to 1.15 eV for the five-ring case, this trend can be seen easily in Fig. 4.19.

The binding energy and other electronic properties of adsorbed molecules are listed in Table 4.2. In addition, the HOMO-CBE energy differences of aromatic rings adsorbed systems for two different anchor group molecules are shown in Fig. 4.21.

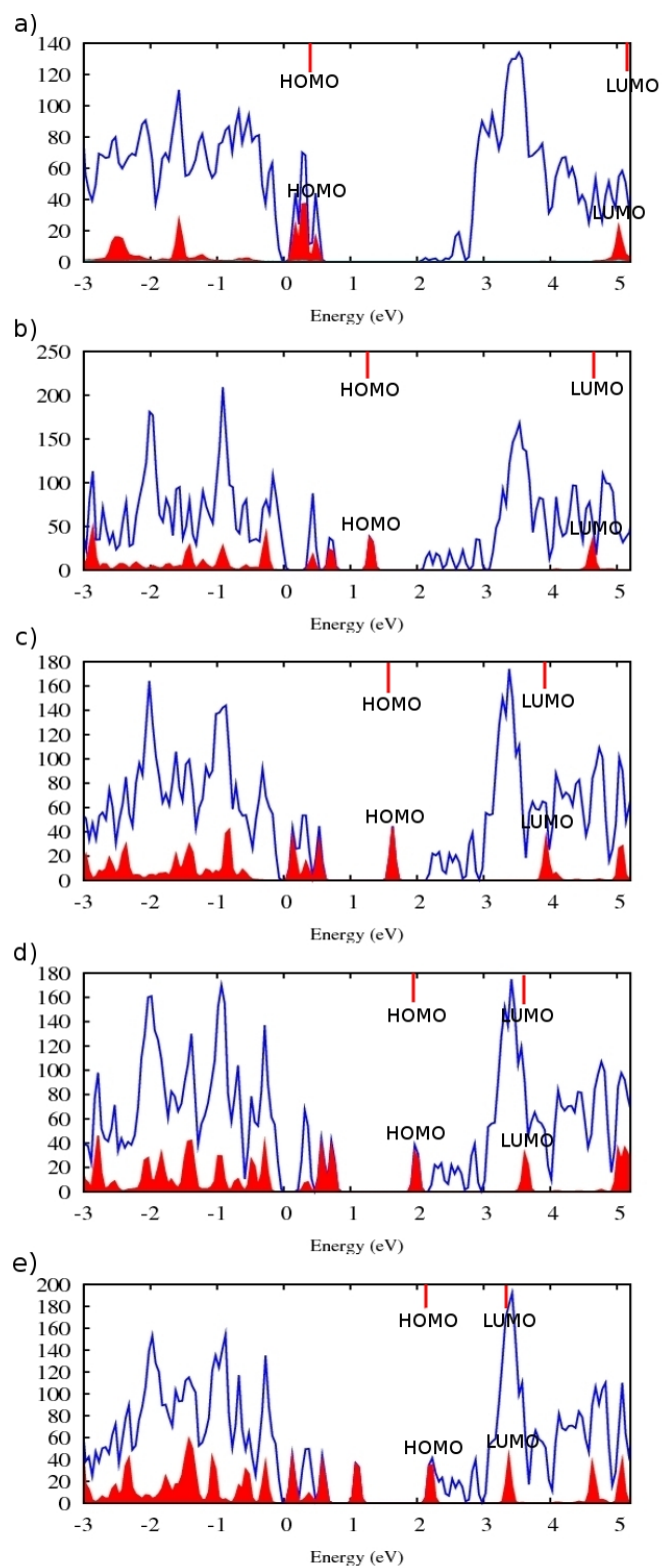


Figure 4.18: Contribution of molecule's partial density of states to the total density of states. Valence band top of the bulk projection is at 0 eV. The number of rings in figure (a), (b), (c), (d), (e) are 1, 2, 3, 4, 5 respectively. The HOMO and the LUMO level of the isolated rings is shown above the each of the panel.

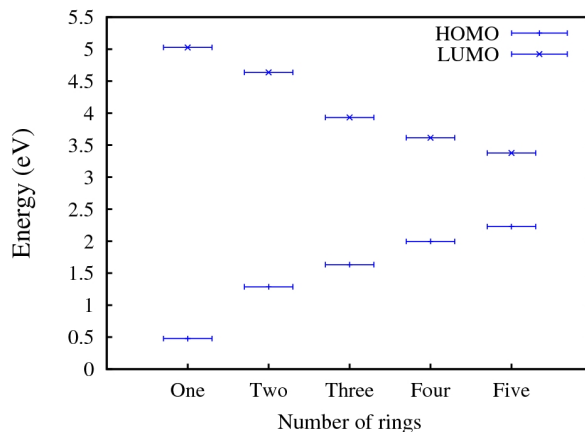


Figure 4.19: HOMO-LUMO energy difference of adsorbed aromatic rings

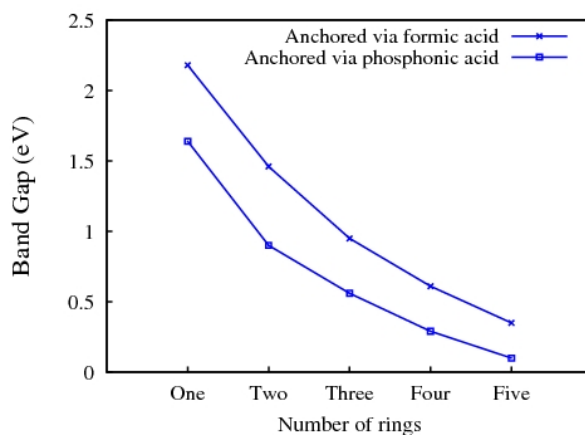


Figure 4.20: Variation energy difference between HOMO-CBE of the systems versus number of rings

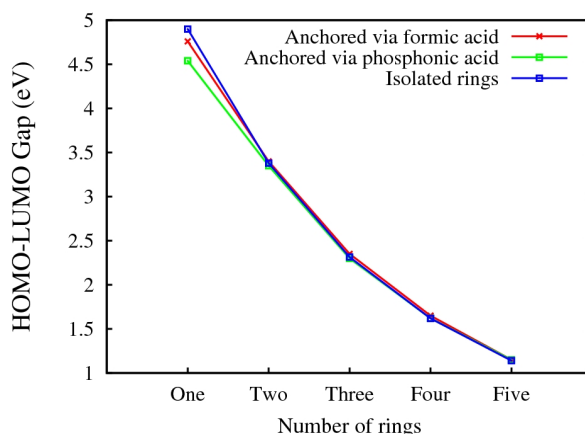


Figure 4.21: Energy difference between HOMO-LUMO gap of the systems versus number of rings

## CHAPTER 5

### CONCLUSION

In this thesis, the electronic structure of aromatic rings, which are the basic building blocks of linear dye molecules, adsorbed on TiO<sub>2</sub> anatase (001) surface is investigated using density functional theory. In experimental applications, dye molecules are adsorbed on the TiO<sub>2</sub> surfaces in order to enable visible light absorption. This study investigates the possibility of visible absorption efficiency enhancement through the adsorption of linear aromatic molecules of varying length. Due to the inertness of aromatic rings, formic (R-COOH) and phosphonic acid molecules (R-PO<sub>3</sub>H<sub>2</sub>), which are the most widely used anchor groups are employed to enable the adsorption. The results indicate that both anchor group molecules are adsorbed on anatase (001) surface with high binding energies although the phosphonic acid is adsorbed on the surface more strongly than the formic acid with a difference of 1.3 eV. In addition, the phosphonic acid causes a narrowing in the band gap of the TiO<sub>2</sub> anatase system, whereas, formic acid does not make any contribution to the band.

Having identified the most favorable adsorption locations for the anchors, linear aromatic molecules comprising one to five rings were attached followed by a geometric relaxation in each case. The geometric structure of the TiO<sub>2</sub> anatase (001) surface were found to be unaffected by the addition of the aromatic molecules. This fact manifests itself in the band structure of the full system where the bands originating from the surface and the adsorbed species are mutually unchanged.

In order to provide a controllable parameter to the design efforts of dye sensitized solar cells (DSSC), the possibility of a trend in the Highest occupied molecular orbital (HOMO) – Lowest unoccupied molecular orbital (LUMO) gap and the HOMO–conduction band edge energy difference was sought. The HOMO–LUMO gap was observed to decrease in a monotonic fashion with increasing ring number. In order to get efficient photovoltaic device the po-

sitions of HOMO and LUMO levels of the molecule are also important in addition to the energy difference between HOMO and the conduction band edge of these systems. The best performance of these systems is achieved when the HOMO level of the molecule is in the band gap so visible light will be absorbed and the LUMO level is in the conduction band of the system so that the excited electron will immediately be passed to the TiO<sub>2</sub> substrate [53]. The positions of the HOMO and LUMO levels of the molecules under consideration are in accordance with this criterion in our work.

All aromatic rings studied in this work have been found to bind strongly to the substrate via the anchor molecules. Furthermore, LUMO levels were observed to be located within the conduction band of the TiO<sub>2</sub> substrate while the HOMO levels display an upward shift with increasing ring number. In light of these findings, the aromatic ring chains were identified as favorable candidates for tunable design of DSSCs. Among the linear chains studied, the most appropriate molecule for use in a single frequency DSSC is likely to be the three-ring chain due to its intermediate size gap. However, the simultaneous use of molecules with varying lengths will have the effect of providing adsorption of a larger portion of the visible spectrum. This conclusion is drawn from the observation of several states introduced in the band gap by each molecule, providing new channels for optical transitions.

## REFERENCES

- [1] U. Diebold, “The surface science of titanium dioxide”, *Surface Science Reports*, vol.48, pp. 53–229, 2003.
- [2] X. Gong, A. Selloni, A. Vittadini, “Density Functional Theory Study of Formic Acid Adsorption on Anatase TiO<sub>2</sub> (001): Geometries, Energetics, and Effects of Coverage, Hydration, and Reconstruction”, *J. Phys. Chem. B*, vol. 110, pp. 2804–2811, 2006.
- [3] H. K. Song, Y. H. Park, C. H. Han, J. G. Jee, “Synthesis of ruthenium complex and its application in dye-sensitized solar cells”, *Journal of Industrial and Engineering Chemistry*, vol. 15, pp. 62–65, 2009.
- [4] C. H. Han, B. Jousseau, M. C. Rascle, T. Toupance, H. Cachet, V. Vivier, “Nanocrystalline F-doped tin dioxide materials: texture, morphology and photosensitization with a perylene-substituted organotin”, *Journal of Fluorine Chemistry*, vol. 125, pp. 1247–1254, 2004.
- [5] B. O’Regan, M. Grätzel, “A low-cost, high-efficiency solar cell based on dye-sensitized colloidal TiO<sub>2</sub> films” *Nature*, vol. 353, pp. 737–740, 1991.
- [6] K. Sayama, K. Hara, N. Mori, M. Satsuki, S. Suga, S. Tsukagoshi, Y. Abe, H. Sugihara, H. Arakawa, “Photosensitization of a porous TiO<sub>2</sub> electrode with merocyanine dyes containing a carboxyl group and a long alkyl chain”, *Chem. Commun.*, pp. 1173–1174, 2000.
- [7] K. Hara, K. Sayama, Y. Ohga, A. Shinpo, S. Suga, H. Arakawa, “A coumarin-derivative dye sensitized nanocrystalline TiO<sub>2</sub> solar cell having a high solar-energy conversion efficiency up to 5.6 %”, *Chem. Commun.*, pp. 569–570, 2001.
- [8] Y. Dai, C. M. Coble, J. Zeng, Y. Sun, Y. Xia, “Synthesis of Anatase TiO<sub>2</sub> Nanocrystals with Exposed [001] Facets”, *Nano Lett.*, vol. 9, no.6, pp. 2455–2459, 2009.
- [9] X. Han, Q. Kuang, M. Jin, Z. Xie, Lansun Zheng, “Synthesis of Titania Nanosheets with a High Percentage of Exposed (001) Facets and Related Photocatalytic Properties”, *J. Am. Chem. Soc.*, vol. 131, no.9, pp. 3152–3153, 2009.
- [10] M. Nilsing, P. Persson, L. Ojamäe, “Anchor group influence on molecule-metal oxide interfaces: Periodic hybrid DFT study of pyridine bound to TiO<sub>2</sub> via carboxylic and phosphonic acid”, *Chemical Physics Letters*, vol. 415, pp. 375–380, 2005.
- [11] K. Capelle, “A Bird’s Eye View of Density Functional Theory”, *Braz. J. Phys.*, vol. 36, no. 4a, 2006.
- [12] R. L. Liboff, “Introductory Quantum Mechanics”, Fourth Edition, Addison Wesley, 2002.
- [13] M. Born, J. R. Oppenheimer, “On the quantum theory of molecules”, *Ann. Physik*, 1927.

- [14] K. Burke, “ABC of DFT”, 2007.
- [15] Micheal Springborg, “Methods of electronic structure calculation”, Cambridge University Press, 2004.
- [16] J. C. Slater, “The Theory of complex spectra”, *Physical Review*, vol. 34, no.10, pp. 1293–1312, 1929.
- [17] P. Hohenberg, W. Khon “Inhomogeneous electron gas”, *Physical Review* 136, B864 1964.
- [18] W. Khon, L. J. Sham, “Self-Consistent Equation Including Exchange and Correlation Effects”, *Physical Review*, vol. 140, pp. 1133–1138, 1964.
- [19] C. Kittel, “Introduction to Solid State Physics”, John Wiley & Sons, Inc., Seventh Edition, 1996.
- [20] R. M. Martin, “Electronic Structure Basic Theory and Practical Methods”, Cambridge University Press, 2004.
- [21] D. R. Hamann, M. Schlüter and C. Chiang, *Phys. Rev. Lett.* vol. 43, pp. 1494–1497, 1979.
- [22] D. Vanderbilt *Physical Review B*, vol. 41, pp. 7892–7895, 1990.
- [23] K. Hashimoto, H. Irea, A. Fujishima, “TiO<sub>2</sub> Photocatalysis: A Historical Overview and Future Prospects”, *Japanese Journal of Applied Physics*, vol. 44, no.12, pp. 8269–8285, 2005.
- [24] T. Morikawa, R. Asahi, T. Ohwaki, K. Aoki, K. Suzuki, Y. Taga, “Visible-light Photocatalyst-Nitrogen-doped Titanium Dioxide”, *R & D Review of Toyota CRDL*, vol. 40, no.3, pp. 45–50, 2005.
- [25] S. Kato, F. Mashio, “Abtr. Book Ann. Meet.”, *Chemical Society of Japan*, p.223, 1956.
- [26] A. Fujishima, K. Honda, “Electrochemical Photolysis of Water at a Semiconductor Electrode”, *Nature*, vol. 238, pp. 37–38, 1972.
- [27] M. R. Hoffmann, S. T. Martin, W. Choi, D. W. Bahneman, “Environmental Applications of Semiconductor Photocatalysis”, *Chemical Review*, vol. 95, pp. 69–96, 1995.
- [28] P. Sawunyama, A. Fujishima, K. Hashimoto, “Observation of a photochemical reaction on the TiO<sub>2</sub> (110) surface by atomic force microscopy”, *J. Phys. Chem. B*, vol. 101, pp. 2229–2230, 1998.
- [29] S. S. Tan, L. Zou, E. Hu, “Photocatalytic reduction of carbon dioxide into gaseous hydrocarbon using TiO<sub>2</sub> pellets”, *Catalysis Today*, vol. 115, pp. 269–273, 2006.
- [30] S. Kayano, T. Watanabe, K. Hashimoto, “Bactericidal Activity of Copper-Deposited TiO<sub>2</sub> Thin Film under Weak UV Light Illumination”, *Environ. Sci. Technol.*, vol. 37, pp. 4785–4789, 2003.
- [31] R. Wang, K. Hashimoto, A. Fujishima, M. Chikuni, E. Kojima, A. Kitamura, M. Shimohigoshi, T. Watanabe, “Photogeneration of Highly Amphiphilic TiO<sub>2</sub> Surfaces”, *Advanced Materials*, vol. 10, pp. 135–138, 1998.

- [32] T. Onoa, T. Yamaguchia, H. Arakawa, “Study on dye-sensitized solar cell using novel infrared dye”, *Solar Energy Materials and Solar Cells*, vol. 93, pp. 831–835, 2009.
- [33] M. Grätzel, “Conversion of sunlight to electric power by nanocrystalline dye-sensitized solar cells”, *Journal of Photochemistry and Photobiology A: Chemistry*, vol. 164, pp. 3–14, 2004.
- [34] E. Borgarello, J. Kiwi, M. Gratzel, E. Pelizzetti, M. Visca, “Visible Light Induced Water Cleavage in Colloidal Solutions of Chromium-Doped Titanium Dioxide Particles”, *J. Am. Chem. Soc.*, vol. 104, pp. 2996–3002, 1982.
- [35] I. Nakamura, N. Negishi, S. Kutsuna, T. Ihara, S. Sugihara, K. Takeuchi, “Role of oxygen vacancy in the plasma-treated TiO<sub>2</sub> photocatalyst with visible light activity for NO removal”, *Journal of Molecular Catalysis A: Chemical*, vol. 161, pp. 205–212, 2000.
- [36] S. Sakthivel, H. Kisch, “Daylight Photocatalysis by Carbon-Modified Titanium Dioxide”, *Angew. Chem. Int. Ed.*, vol. 42, pp. 4908–4911, 2003.
- [37] S. Sakthivel, M. Janczarek, H. Kisch, “Visible Light Activity and Photoelectrochemical Properties of Nitrogen-Doped TiO<sub>2</sub>”, *J. Phys. Chem. B*, vol. 108, pp. 19384–19387, 2004.
- [38] H. Irie, S. Washizuka, N. Yoshinob, K. Hashimoto, “Visible-light induced hydrophilicity on nitrogen-substituted titanium dioxide films”, *Chem. Commun.*, pp. 1298–1299, 2003.
- [39] F.A. Grant, “Properties of Rutile(Titanium Dioxide)”, *Reviews of Modern Physics*, vol. 31, no.3, pp. 646–673, 1959.
- [40] A.E. Goresy, M.Chen, L. Dubrovinsky, P. Gillet, G. Graup, “An Ultradense Polymorph of Rutile with Seven-Coordinated Titanium from the Ries Crater”, *Science*, vol. 293, pp. 1467–1470, 2001.
- [41] A.E. Goresy, M.Chen, P. Gillet, L. Dubrovinsky, G. Graup, R. Ahuja, “A natural shock-induced dense polymorph of rutile with  $\alpha$ -PbO<sub>2</sub> structure in the suevite from the Ries crater in Germany”, *Earth and Planetary Science Letters*, vol. 192, pp. 485–495, 2001.
- [42] N. N. Greenwood, A.Earnshaw, *Chemistry of the Elements*, Oxford Press.
- [43] M. Ramamoorthy, D.Vanderbilt, First-principles calculations of the energetics of stoichiometric TiO<sub>2</sub> surfaces, *Physical Review B*, vol. 49, no.23, pp. 16721–16727, 1994.
- [44] T. Ohno, K. Sarukawa, K. Tokieda, M. Matsumura, “Morphology of a TiO<sub>2</sub> Photocatalyst (Degussa, P-25) Consisting of Anatase and Rutile Crystalline Phases”, *Journal of Catalysis*, vol. 203, pp. 82–86, 2001.
- [45] K. Sayama, H. Sugihara, H. Arakawa, “Photoelectrochemical Properties of a Porous Nb<sub>2</sub>O<sub>5</sub> Electrode Sensitized by a Ruthenium Dye”, *Chem. Mater.*, vol. 10, no.12, pp. 3825–3832, 1998.
- [46] S. K. Deb. “Dye-sensitized TiO<sub>2</sub> thin-film solar cell research at the National Renewable Energy Laboratory (NREL)”, *Solar Energy Materials and Solar Cells*, vol. 88, pp. 1–10, 2005.

- [47] R. M. Wentzcovitch, J. L. Martins, G. D. Price, “Ab-initio Molecular-Dynamics with Variable Cell Shape-application to  $\text{MgSiO}_3$ ”, *Physical Rev. Lett.*, vol. 70, pp. 3947–3950, 1993.
- [48] Computations have been carried out with the PWSCF-ESPRESSO software, GNU General Public Licence.
- [49] J. P. Perdew, K. Burke, M. Ernzerhof. “Generalized gradient approximation made simple”, *Physical Rev. Lett.*, vol. 77, pp. 3865–3868, 1996.
- [50] R. Luschtinetz, J. Frenzel, T. Milek, G. Seifert, “Adsorption of Phosphonic Acid at the  $\text{TiO}_2$  Anatase (101) and Rutile (110) Surfaces”, *J. Phys. Chem. C*, vol. 113, pp. 5730–5740, 2009.
- [51] J. Schnadt, P. A. Brühwiler, L. Patthey, J. N. O’Shea<sup>1</sup>, S. Södergren, M. Odellius, R. Ahuja<sup>1</sup>, O. Karis, M. Bäessler, P. Persson, H. Siegbahn, S. Lunell, N. Martensson, “Experimental evidence for sub-3-fs charge transfer from an aromatic adsorbate to a semiconductor”, *Nature*, vol. 418, pp. 620–623, 2002.
- [52] M. Nilsing, S. Lunell, P. Persson, L. Ojamäe “Phosphonic acid adsorption at the  $\text{TiO}_2$  anatase [101] surface investigated by periodic hybrid HF-DFT computations”, *Surface Science*, vol. 582, pp. 49–60, 2005.
- [53] S. Meng, J. Ren, E. Kaxiras, “Natural Dyes Adsorbed on  $\text{TiO}_2$  Nanowire for Photovoltaic Applications: Enhanced Light Absorption and Ultrafast Electron Injection”, *Nano Letters*, vol. 8, pp. 3266–3272, 2008.